Study on multi-species hydrocarbon detection using tunable diode laser absorption spectroscopy

Mechanical engineering

Intelligent structures and mechanics system engineering

Graduate School of Advanced Technology and Science

Tokushima University

Qiming Wang

Supervisor：Prof. Deguchi

September 2021

Abstract

Tunable diode laser absorption spectroscopy (TDLAS) is a widely used diagnostic technique due to its high sensitivity, fast response, low cost, and other merits. Hydrocarbon detection is a field of great interest in the application of tunable diode lasers as hydrocarbons are fundamental molecules in many industrial processes. Many tunable diode lasers are only suitable for single species detection due to the short scanning range and in real situations. However, different hydrocarbon species tend to exist simultaneously.

Here we present a laser system based on the difference-frequency generation (DFG) method for simultaneous hydrocarbon mixtures detection. The direct absorption spectra of different hydrocarbons covering various groups (e.g., alkane, olefin, and aromatic) were measured. The measurements of the concentration dependence of absorbance for each molecule were carried out. The R^2 values were larger than 0.997, which demonstrated the system can measure hydrocarbons covering different molecular classes accurately. The mixture components were identified using the independent component analysis and quantitative analysis were performed using the classical least-squares method. The analysis of different types of mixture measurements proved the capability of multi-species hydrocarbon detection.

Two actual validation experiments were also performed. In the low temperature coal pyrolysis experiment, the coal sample was heated up to 350℃ and the recorded spectra were analyzed by comparing with the pure hydrocarbon spectra database. A least-squares fitting was performed to quantitatively determine the concentration of each component within the mixture. Totally eleven different species were identified and the R^2 values close to 1 indicates the variance between measured and fitted data was small. In the engine exhaust experiment, the spectra of engine exhaust were recorded and analyzed using the same method. Hydrocarbon from C_3-C_8 and small amount of methane were recognized. The concentration variation with time was also observed.

Overall, the proposed system is a good candidate for industrial hydrocarbon detection by overcoming the limitation of other tunable diode lasers designed for hydrocarbon measurement while maintaining its advantages. The two actual experiments proved the proposed laser system can detect multiple hydrocarbons simultaneously in actual situations.

Keywords: Hydrocarbon measurement; Tunable diode laser absorption spectroscopy (TDLAS); difference frequency generation (DFG), Coal pyrolysis; Engine exhaust;

Table of contents

Abstract 2

1 Introduction 5

1.1 Background of study 5

1.2 Tunable diode laser and research status 5

2 Theory 8

2.1 Absorption Spectroscopy 8

2.2 Absorption line strength 8

2.2 Broadening function 9

2.3 Data analysis 10

3 Experiment method 12

3.1 DFG laser system 12

3.2 Gas phase hydrocarbon measurement using TDLAS 13

3.3 Vapor phase hydrocarbon measurement using TDLAS 14

3.4 Vapor phase hydrocarbon measurement using external-cavity diode laser 16

3.5 Engine exhaust measurement using TDLAS 18

3.6 Low-temperature coal pyrolysis process measurement using TDLAS 19

4 Results and discussion 21

4.1 Laser performance 21

4.2 Single and mixture hydrocarbon measurement result 23

4.2.1 single species measurement 23

4.2.2 single species measurement using the ECD laser 41

4.2.3 signal to noise ratio and limit of detection 43

4.2.4 mixture measurement analysis using one wavelength 44

4.2.5 mixture measurement analysis using ICA and CLS methods 49

4.3 Engine exhaust measurement result 54

4.4 Low-temperature coal pyrolysis process measurement result 57

5 Conclusions 61

1) Hydrocarbon measurement using a DFG laser 61

2) Engine exhaust measurement 61

3) Coal powder measurement 61

References 63

Acknowledgments 70

1 Introduction

1.1 Background of study

Hydrocarbon is a common chemical compound, and its detection is a broadly discussed topic in various fields ranging from fundamental research to industrial application. In the coal industry, most coal conversion processes like combustion, gasification, and liquefaction, pyrolysis (or devolatilization) is an important initial step [1]. The volatiles and tars released during this step accounts for up to 70% of the weight loss [2]. As a major composition in the gaseous product, the hydrocarbon releasing characteristics are important for pollution control and clarification of the pyrolysis mechanism. Common measurement instruments and methods applied in the coal pyrolysis process detection include gas chromatography (GC), mass spectrum (MS), thermogravimetric (TG), Fourier transform infrared spectrometer (FTIR) and their combinations [3]–[6]. Most of these methods require pretreatment and isolation process [7] and is hard to achieve real-time and in-situ hydrocarbon measurement.

Hydrocarbon species contain a C-H bond that has a fundamental vibrational mode. The C-H stretch results in many absorption bands in 3μm and 10μm, making these regions easy for hydrocarbon measurement. Many previous works that measure hydrocarbons fall into the near-infrared to mid-infrared region (2.5-12μm). Detection of methane [8], ethane [9], and propane [10] were performed using various DFB lasers. Quantum cascade lasers (QCL) and interband cascade lasers (ICL) also provide new opportunities for hydrocarbon detection [11]–[15]. Several tunable lasers based on difference-frequency generation were developed to measure methane as well as hydrocarbon fuel components detection [16]–[21]. Despite the benefits and wide application, most TDLAS techniques are designed to measure specific target gas due to their narrow spectral range limitation. Also, spectrally isolated features were required for quantitative measurements thus need fine-tuning for the desired wavelength. The limitation on the simultaneous measurable hydrocarbon species poses obstacles to the application of laser absorption spectroscopy. This makes the TDLAS method less appealing when compared to other broad range detection methods like the Fourier-transform infrared spectroscopy (FTIR) [3], thermogravimetric analysis–mass spectrometry (TG-MS) [4], or coupled with gas chromatography [5], or their combination [6].

1.2 Tunable diode laser and research status

Tunable diode laser covers a large variety of lasers with different wavelength range, as can be seen from Fig. 1.1.

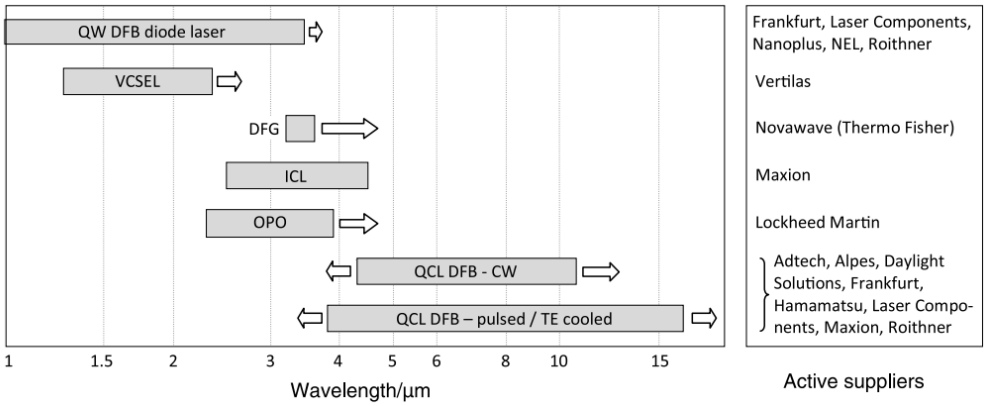

Fig. 1.1 Wavelength coverage for tunable lasers in IR (about 1μm) and its suppliers [22]

DFB lasers and Vertical-Cavity Surface-Emitting Lasers (VCSEL) are widely used in near infrared region. But DFB lasers usually have short tuning range, so wavelength selection is required for mode-hop free single-mode operation. The merits of VCSEL are fast tuning speed (over 1GHz), low threshold and low noise, high conversion efficiency and low power consumption, low-cost while demerits are low output power.

DFG laser consists of two seed lasers, one is pump laser which has high power, and another is tunable laser with lower power. Two laser beams are combined to produce final output. A review of DFG laser is written by Richter et al [23]. DFG laser has the merits of narrow output beam broadening width, high spectrum purity and can achieve high sensitivity gas sensing in normal temperature. But power output of DFG laser is usually small due to low efficiency of difference frequency.

ICL operates in range between 2.5 to 4μm and covers the gap between diode laser and QCL. But compared to QCL, ICLs are less matured and fewer instrument developments were achieved.

Optical parametric oscillator (OPO) converts input laser wave into two output waves with lower frequency [24]. Compared to DFG lasers, OPOs are sensitive to mechanical or thermal instability.

QCL was invented in 1994. Wavelength range for quantum cascade laser fall in 3.5 to 24μm which creates new opportunities for various gas detection. A review of QCL can be found in [25].

Tunable diode laser absorption spectroscopy has many merits compare to traditional gas sensing methods. Its high sensitivity, fast response, reasonable costs compare to other laser diagnostic

techniques enable its application to various areas of science and industry. For example, in high resolution molecular spectroscopy [25]–[29], trace gas analysis [30]–[32], plasma diagnostics [33], [34], combustion diagnostics [35]–[37] and so on. TDLAS has the potential to be applied in both the study of industrial process phenomena and in situ monitoring and control of industrial systems.

2 Theory

2.1 Absorption Spectroscopy

TDLAS follows Beer-Lambert's law. According to this law, when light permeates an absorption medium, the molecular concentration is proportional to the strength of the transmitted light. Relationship between the number density of measured species and amount of light absorbed can be explained by following formula:

$$\frac{I_\lambda}{I_0} = \exp\{-A_\lambda\} = \exp\{-\sum_i (n_i L \sum_j S_{i,j}(T) G_{vi,j})\} \qquad (2.1)$$

Where I_λ and I_0 represents incident and transmitted light intensity, respectively. A_λ is absorbance, n_i is number density of species i, L is path length, $S_{i,j}$ is absorption line strength of absorption line j and $G_{vi,j}$ is line broadening function.

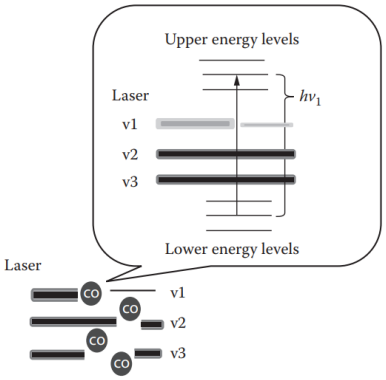

Fig. 2.1 Energy transfer process of TDLAS [38]

From this formula we can infer that absorbance of a mixture is the linear combination of absorbances of the components.

In this study, absorbance spectra of different hydrocarbon species (both singular and plural) were used to conduct quantitative analysis of concentration and temperature.

2.2 Absorption line strength

Absorption line strength $S_{i,j}$ represents the degree of light intensity absorption of that line, which is the outcome of absorption and emission when molecules' transition take place. Line strength only relates to temperature and can be calculated using HITRAN database [39]. Line strength at temperature T is shown as the following formula:

$$S_{i,j}(T) = S(T_0)\frac{Q(T_0)}{Q(T)}\exp\left[-\frac{hcE_i''}{k}\left(\frac{1}{T}-\frac{1}{T_0}\right)\right]\times\left[\frac{1-\exp(-\frac{hc\nu_0}{kT})}{1-\exp(-\frac{hc\nu_0}{kT_0})}\right] \qquad (2.2)$$

Where T_0 represents reference temperature, Q is partition function, E_i'' is energy in low transition state, h is Planck constant, k is Boltzmann constant, c is light speed and ν_0 is transition frequency. By applying polynomial fitting, Q can be written as:

$$Q(T_j) = a + bT_j + cT_j^2 + dT_j^3 \qquad (2.3)$$

Where coefficient a, b, c, d varies according to different gas and temperature range and can also refer to HITRAN database.

2.2 Broadening function

Theoretically, absorption spectrum lines should have infinitely sharpness. However, due to thermal motion and collision among the particles, those lines have particular shapes. Broadening can be categorized as homogeneous broadening and inhomogeneous broadening. The former affects every molecule in the same way and the latter results from different molecules have various resonant frequencies [40]. Homogeneous broadening consists of natural broadening and collisional broadening, while inhomogeneous consists of doppler broadening. The effect of natural broadening is small, so broadening is dominated by collisional and doppler broadening.

To describe broadening effects, several broadening functions can be applied under different conditions.

1) Lorentzian line shape function

When pressure effects more in measurement, line shape can be described using Lorentzian function, which can be written as:

$$G_c(\nu) = \frac{1}{2\pi}\frac{\Delta\nu_c}{(\upsilon-\nu_0)^2(\frac{\Delta\nu_c}{2})^2} \qquad (2.4)$$

Where $\Delta\nu_c$ means full width at half maximum (FWHM) of collisional broadening, υ is frequency of light and ν_0 the transition center frequency.

2) Gaussian line shape function

When thermal effect dominates measurement environment over pressure, Gaussian function can be applied which is written as:

$$G_D(\nu) = \frac{2}{\Delta\nu_D}(\frac{ln2}{\Pi})^{1/2}\exp\{(-4ln2\frac{\nu-\nu_0}{\Delta\nu_D})^2\} \qquad (2.4)$$

$$\Delta\nu_D = (7.1623\times10^{-7})\nu_0\sqrt{\frac{T}{M}} \qquad (2.5)$$

Where $\Delta\nu_D$ is FWHM of doppler broadening, T is absolute temperature and M is molar mass.

3) Voigt line shape function

When doppler broadening and collisional broadening both have effects, it is better to use Voigt function, which can be written as:

$$G_V(a,x) = \int_{-\infty}^{+\infty} G_D(u)G_C(V-u)du = G_D(\nu_0)\frac{a}{\pi}\int_{-\infty}^{+\infty}\frac{\exp(-y^2)}{a^2+(x-y)^2}dy \quad (2.6)$$

$$a = \sqrt{\ln 2}\frac{\Delta\nu_c}{\Delta\nu_D} \quad (2.7)$$

$$x = \sqrt{\ln 2}\frac{(\nu-\nu_0)}{\Delta\nu_D} \quad (2.8)$$

$$\Delta\nu_V = \frac{\Delta\nu_c}{2} + \sqrt{(\frac{\Delta\nu_c}{4} + {\Delta\nu_D}^2)} \quad (2.9)$$

By far, it is unable to analytical expression of convolution calculation. Much research has been done on solving Voigt function. Some important algorithms are proposed by Drayson [41], Wells [42], and Whiting [43].

2.3 Data analysis

In this research, two methods were applied for data analysis, namely the independent component analysis (ICA) and the classical least-squares (CLS) method.

The independent component analysis (ICA) is a signal processing method for signal separation and has been applied for chemometrics usage (mixture decomposition) by many researchers [44]–[46]. In real situations, a common scenario is that only the spectra of the mixtures are available. In the signal processing field, this is known as the "blind separation problem" or the blind separation of sources (BSS) when signals from multiple sources are mixed and need to be deconvolved [47]. The ICA method can restore the original source signal from a set of observed signals which contains the mixed spectra information by decomposing a multisensory data matrix into a linear mixture of a priori unknown source signals. Due to the lack of both the source signals and mixing information, there are two important restrictions when applying the ICA method [48]:

1) The components of the source signal need to be statistically independent.

2) At most one component of the source signal obeys the Gaussian distribution.

The linear ICA problem can be expressed as:

$$\boldsymbol{X} = \boldsymbol{AS} \quad (2.10)$$

where $\boldsymbol{X}$ is a M×N matrix of the measured mixture spectra, $\boldsymbol{S}$ is a K×N matrix of K unknown spectra of pure components, and $\boldsymbol{A}$ is a M×K mixture matrix (unknown concentration). The ICA

approach tries to find the optimal separation matrix $\boldsymbol{W}$ to make the components of $\boldsymbol{Y}$ as independent as possible.

$$\boldsymbol{Y} = \boldsymbol{MX} = \boldsymbol{W^T X} \qquad (2.11)$$

In this work, the FastICA [49] algorithm was applied for components identification due to its fast speed.

To determine the concentrations for each component in a mixture, the classical least-squares (CLS) method was applied. It is a well-known regression method and can be applied directly to quantitative spectral analysis.

Another way of representing the Beer-Lambert law for multiple components at a single wavelength is given by the following equation:

$$A = \sum_i^n k_i \, c_i \qquad (2.12)$$

where A is the absorbance of the mixture at a given wavelength, k_i is the absorbance coefficient and c_i is the concentration of the pure substance. By expanding this formula to multiple wavelengths, the following matrix equation can be obtained:

$$\boldsymbol{A} = \boldsymbol{KC} \qquad (2.13)$$

where $\boldsymbol{A}$ is the absorbance matrix of the mixture, $\boldsymbol{K}$ is a matrix of the pure component spectra making up the mixture, and $\boldsymbol{C}$ is a single column matrix of concentration. The idea of this method is to find the concentration for each component that minimizes the sum of the squares of the errors $\boldsymbol{A} - \boldsymbol{KC}$, and the calculated $\boldsymbol{C}$ will then be the best least-squares solution for equation (5).

The Euclidean norm of the errors can be written as:

$$\|\boldsymbol{A} - \boldsymbol{KC}\|_2^2 = \boldsymbol{C}^T\boldsymbol{K}^T\boldsymbol{KC} - 2\boldsymbol{A}^T\boldsymbol{KC} + \boldsymbol{A}^T\boldsymbol{A} \qquad (2.14)$$

By setting the expression to zero and performing matrix multiplications, the concentrations of components in the mixture were calculated the following equation:

$$\boldsymbol{C} = (\boldsymbol{K}^T\boldsymbol{K})^{-1}\boldsymbol{K}^T\boldsymbol{A} \qquad (2.15)$$

More detailed information on this method and the derivation of the equation was discussed in [50].

3 Experiment method

The experiments being carried out can be categorized into two groups, one is the basic experiments, in which the pure spectra were measured using different setups. Another is the application experiments which consists of the engine exhaust measurement and the coal pyrolysis measurement. In this section, the experiment setups and the experiment conditions were discussed.

3.1 DFG laser system

Figure 3.1 displays the outline of the laser system. Two seed lasers sources, an external cavity diode laser (HSL-1-10-40-ZZ-Z-T-P, Stantec co.), which served as the signal source, and a DFB laser (DFB laser was placed inside the DFG module), which served as the pump source, were combined and transferred to the DFG laser conversion module (WD-3236/3250-001-A-A-E, NTT Electronics co.) to generate the idler laser beam. The DFB laser was placed inside the DFG laser conversion module. The beam of the DFB laser was amplified using an amplifier (FA1550QLS, NTT Electronics co.) before the combination with the signal source. The power of the idler wave is at the level of μw and the sweep span of the laser system is over 130nm with a sampling rate of 6kHz.

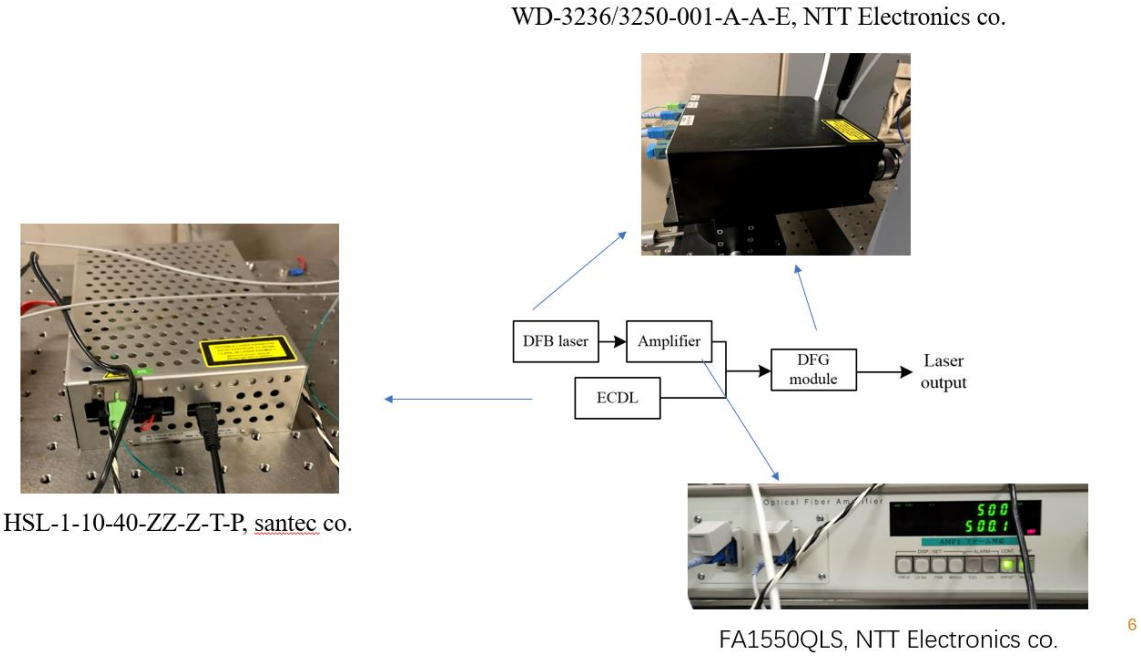

Fig. 3.1 DFG laser system

3.2 Gas phase hydrocarbon measurement using TDLAS

Figure 3.2 is a schematic drawing of the experimental setup for the measurement of hydrocarbons in their gas phase. Hydrocarbon and nitrogen gases were metered through independent mass flow controllers (FCST1005MZF-4J2-F1L-N2-R4, Fujikin Co., Ltd.) before mixing. The concentrations of hydrocarbon molecules were adjusted by controlling the flow rate of hydrocarbon and nitrogen gases. Gas pipes were wrapped with electrical heating tapes that were connected to temperature controllers for temperature adjustment. Heat isolation materials were covered outside gas pipes for heat reservation. Orange blocks represent the parts of the setup that can be heated. The mixed gas flowed through an absorbing cell with a laser path length of 100mm. The absorbing cell was placed inside an electrical heating furnace which was also connected to a temperature controller. Signals from the DFG laser were detected by an infrared detector (PVI-3TE-5-1x1-T08-wBaF2-35, VIGO System S.A.) with a built-in preamplifier model (MIP-DC-20M-F-M4, VIGO System S.A.). The signals were then recorded by an oscilloscope with a 125MHz bandwidth and a total recording time of 200ms (PicoScope 5444B, Pico Technology). The resolution of the system is around 0.01cm^{-1}.

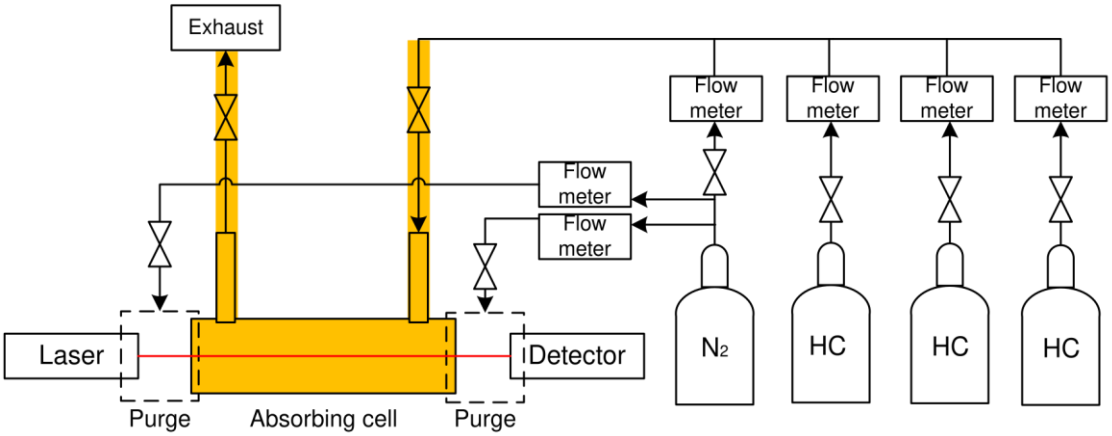

Fig. 3.2 Gas phase hydrocarbon measurement experiment setup

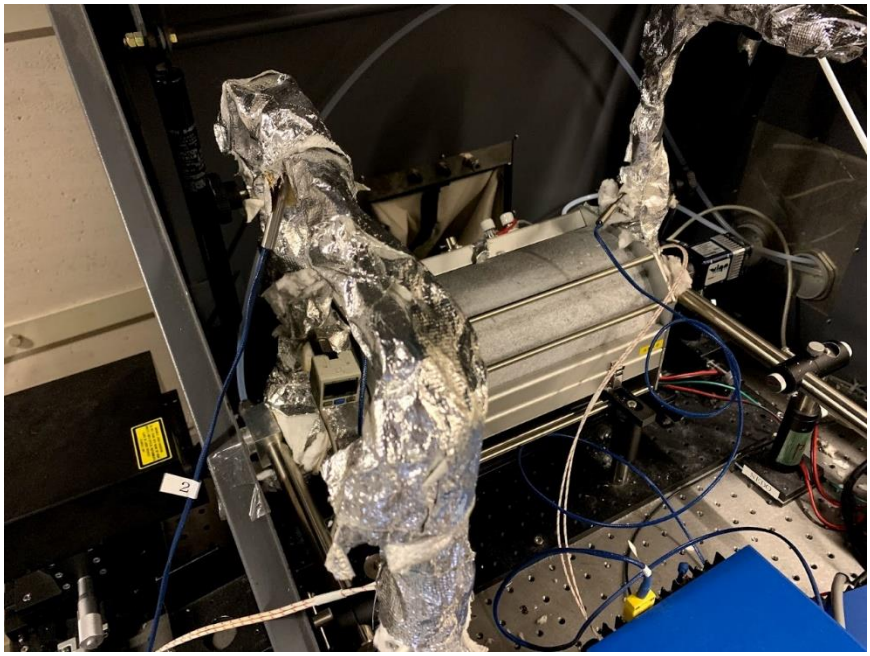

Fig. 3.3 photo of laser, absorbing cell and detector

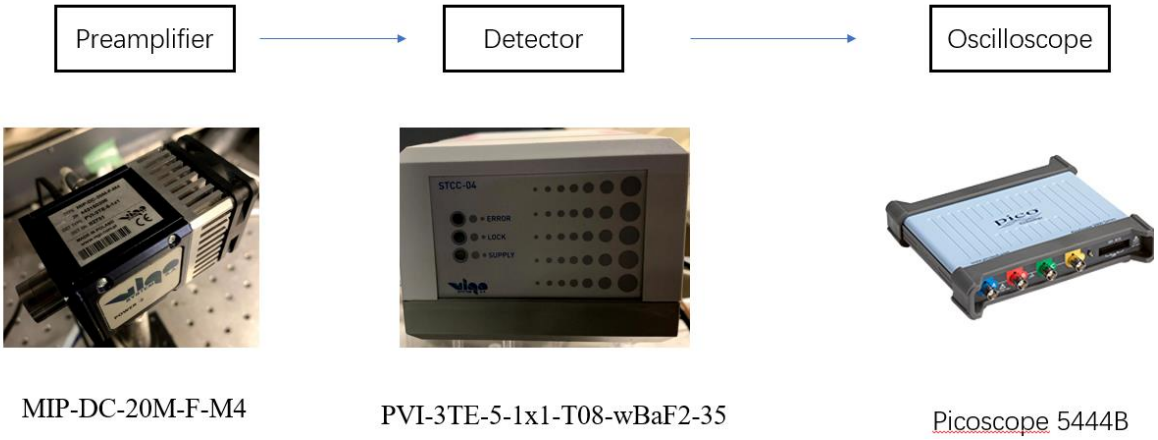

Fig. 3.4 detection system

Figure 3.3 and Fig. 3.4 were the photos of the whole measurement system and the detection system, respectively.

3.3 Vapor phase hydrocarbon measurement using TDLAS

Some heavy hydrocarbons were in the liquid phase under room temperature and need to be heated to the gas phase before measuring. Fig. 3.5 illustrates the outline of the experimental setup for these hydrocarbons. Most parts of the system were the same as the gas phase measurement setup. A single syringe infusion pump (KDS-100, ISIS Co., Ltd.) was used instead of gas cylinders. A syringe was placed above the pump, and the concentration of liquid hydrocarbons was adjusted

by changing the injection speed of the syringe. Liquids were injected into a heating chamber to make sure it was fully vaporized before entering the absorbing cell and another cell was used as a container at the exit to collect condensed hydrocarbon.

Fifteen hydrocarbons were chosen to cover various hydrocarbon classes and the different number of carbon atoms ranging from C_1 to C_8. The straight alkanes studied were methane (CH_4), ethane (C_2H_6), propane (C_3H_8), n-butane (C_4H_{10}), n-pentane (C_5H_{12}), n-hexane (C_6H_{14}), and n-heptane (C_7H_{16}). Two straight alkenes chosen were ethene (C_2H_4) and propene (C_3H_6). Benzene (C_6H_6), toluene (C_7H_8), and m-xylene (C_8H_{10}) were picked for aromatics. Three species belonging to other classes were methylcyclohexane (C_7H_{14}), diisobutylene (C_8H_{16}), and isooctane (C_8H_{18}), which are common components of gasoline surrogate fuels [51].

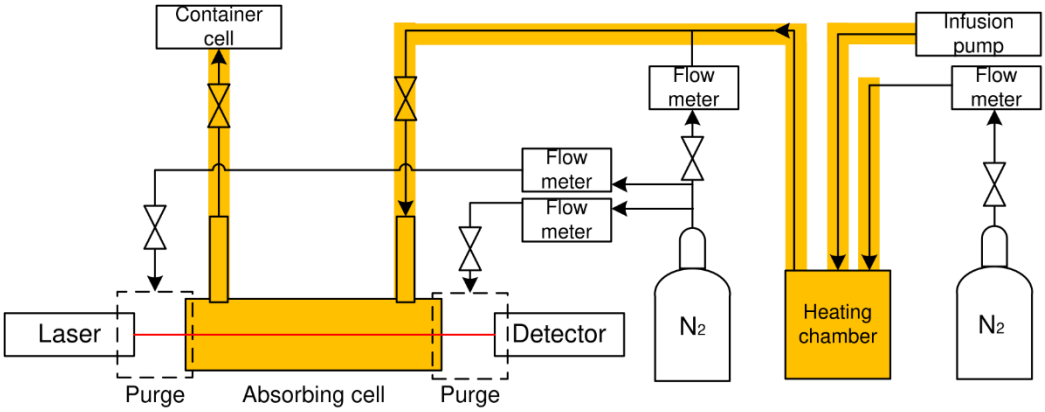

Fig. 3.5 Vapor phase hydrocarbon measurement experiment setup

Table 1 summarized the chosen single molecules and their experimental conditions. Hydrocarbon molecules with over five carbon atoms were measured in their vapor phase under higher temperature conditions (423K) using the vapor phase experiment setup. Others were measured using the gas phase setup. All experiments were performed under ambient pressure. When performing the experiments, the pure nitrogen spectra were first recorded as the baseline, then the hydrocarbon/nitrogen mixture spectra were recorded to calculate absorption spectra using Beer-Lambert's law. The details on data processing was discussed in the next chapter.

Table 1 Experimental conditions for single species

Species	Molecular Class	Concentration	Temperature	Measurement Phase
Methane (CH_4)	Straight alkane	0.12%-0.58%	293-723K	Gas
Ethene (C_2H_4)	Straight alkene	0.09%-0.99%	293-723K	Gas
Ethane (C_2H_6)	Straight alkane	0.05%-0.20%	293-723K	Gas
Propene (C_3H_6)	Straight alkene	0.09%-0.98%	293-723K	Gas
Propane (C_3H_8)	Straight alkane	0.08%-0.39%	293-723K	Gas
n-Butane (C_4H_{10})	Straight alkane	0.06%-0.49%	293-723K	Gas
n-Pentane (C_5H_{12})	Straight alkane	0.42%-1.26%	423-723K	Vapor
n-Hexane (C_6H_{14})	Straight alkane	0.37%-1.10%	423-723K	Vapor
Methylcyclohexane (C_7H_{14})	Alkylcycloalkanes	1.14%-1.88%	423-723K	Vapor
n-Heptane (C_7H_{16})	Straight alkane	0.33%-0.99%	423-723K	Vapor
Diisobutylene (C_8H_{16})	Branched alkene	0.31%-0.93%	423-723K	Vapor
Isooctane (C_8H_{18})	Branched alkane	0.30%-0.88%	423-723K	Vapor
Benzene (C_6H_6)	Aromatic	1.09%-2.15%	423-723K	Vapor
Toluene (C_7H_8)	Aromatic	1.36%-2.24%	423-723K	Vapor
m-Xylene (C_8H_{10})	Aromatic	0.79%-1.56%	423-723K	Vapor
Naphthalene ($C_{10}H_8$)	Aromatic	1.02%	523-723K	Vapor

3.4 Vapor phase hydrocarbon measurement using external-cavity diode laser

For comparison with the DFG laser, another external-cavity diode laser (ECDL) was used for some vapor phase hydrocarbons. Fig. 3.6 and Fig. 3.7 displayed the outline of the system and the photo of the system, respectively.

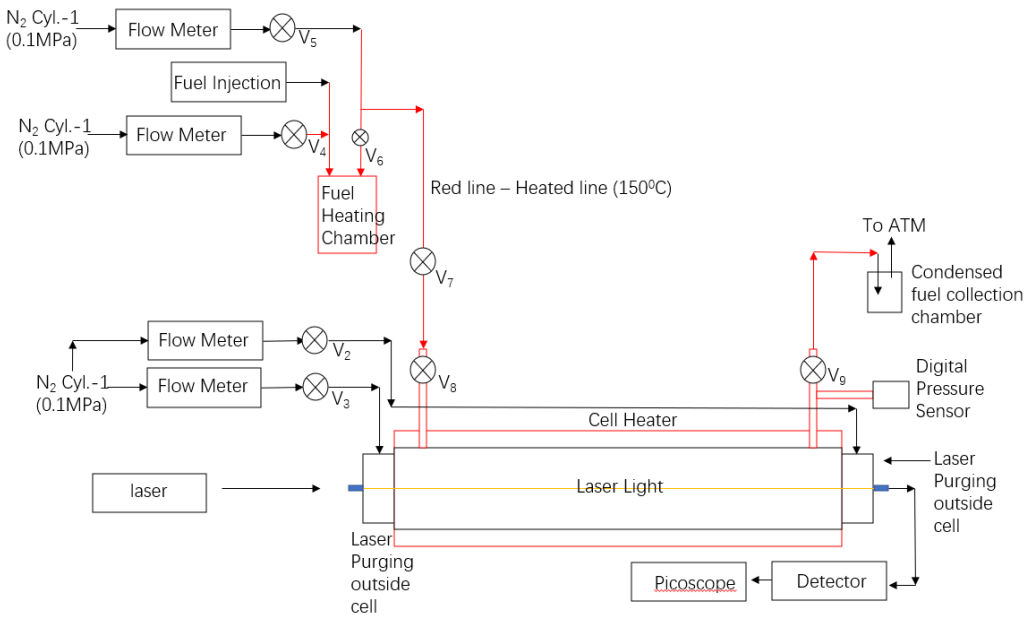

Fig. 3.6 Vapor phase hydrocarbon measurement experiment setup using the ECDL

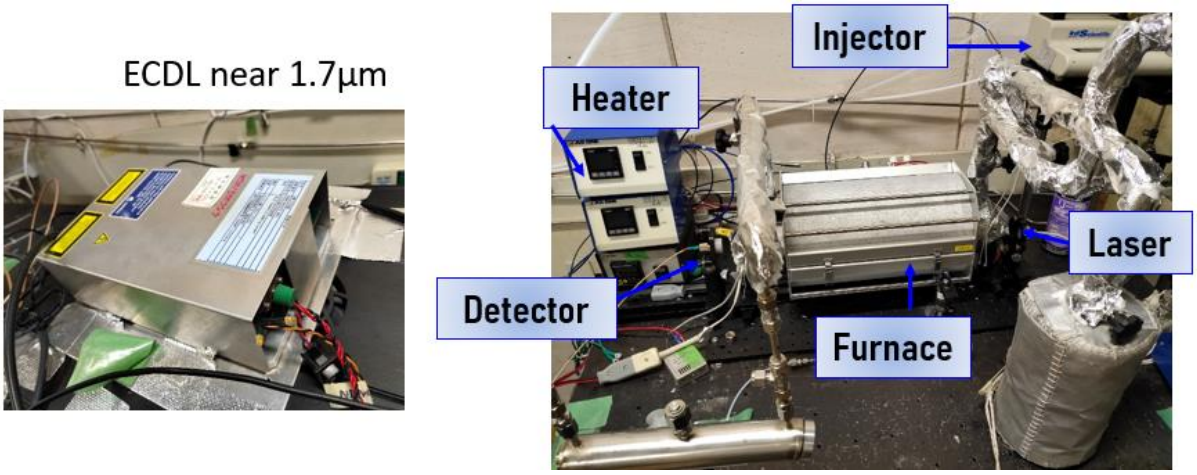

Fig. 3.7 photo of the measurement system using the ECDL

The experimental conditions using the ECDL system was summarized in Table 2.

Table 2 Experimental conditions using the ECDL system

Species	Molecular Class	Concentration	Temperature	Measurement Phase
Methylcyclohexane (C_7H_{14})	Alkylcycloalkanes	5.95%-15.35%	423K-723K	Vapor
n-Heptane (C_7H_{16})	Straight alkane	5.22%-13.63%	423K-723K	Vapor
Diisobutylene (C_8H_{16})	Branched alkene	4.90%-12.87%	423K-723K	Vapor
Isooctane (C_8H_{18})	Branched alkane	4.66%-12.29%	423K-723K	Vapor
Toluene (C_7H_8)	Aromatic	7.04%-17.84%	423K-723K	Vapor

3.5 Engine exhaust measurement using TDLAS

Experimental setup is shown in Fig. 3.4. Laser and detector are placed 5mm above engine exhaust pipe (FUJI HEAVY INDUSTRIES, Inc.， EX17-2BS). Despite DFG laser, another DFB laser (NLK1E5GAAA, NTT Electronics co.) operating at 1388nm with scan range of 0.6nm is used for water vapor absorption spectrum detection to measure temperature. Two lasers were placed as a cross shape. Diameter of engine exhaust pipe is 45mm with 3.5mm thickness and 160mm length. A thermocouple (KMT-100-100-120, Anbe SMT Co.) is also placed in the center of exhaust pipe exit. One rotation speed tester (FT3406, HIOKI TACHO HiTESTER) was placed near engine for rotation speed testing.

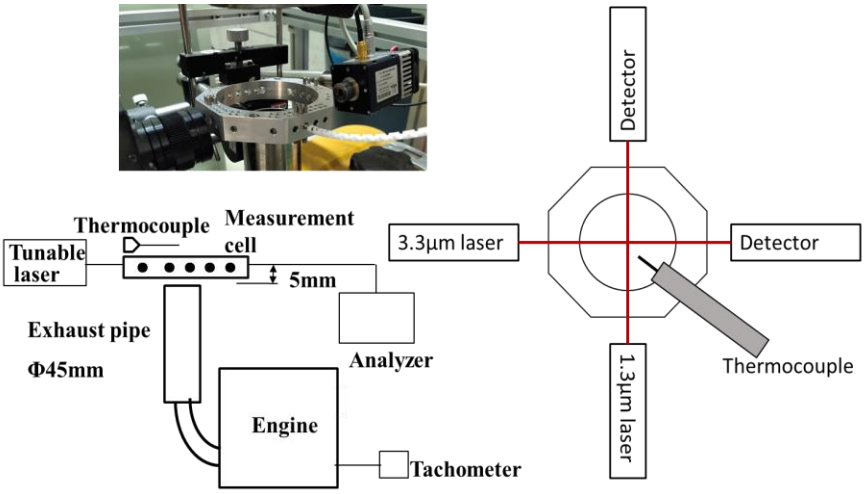

Fig. 3.8 Engine exhaust measurement setup

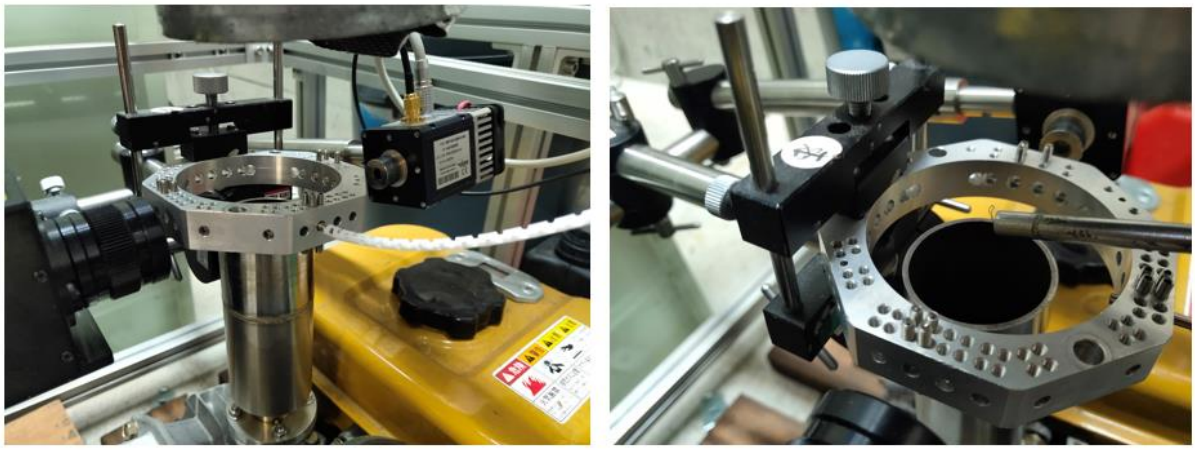

Fig. 3.9 Engine exhaust measurement setup photo

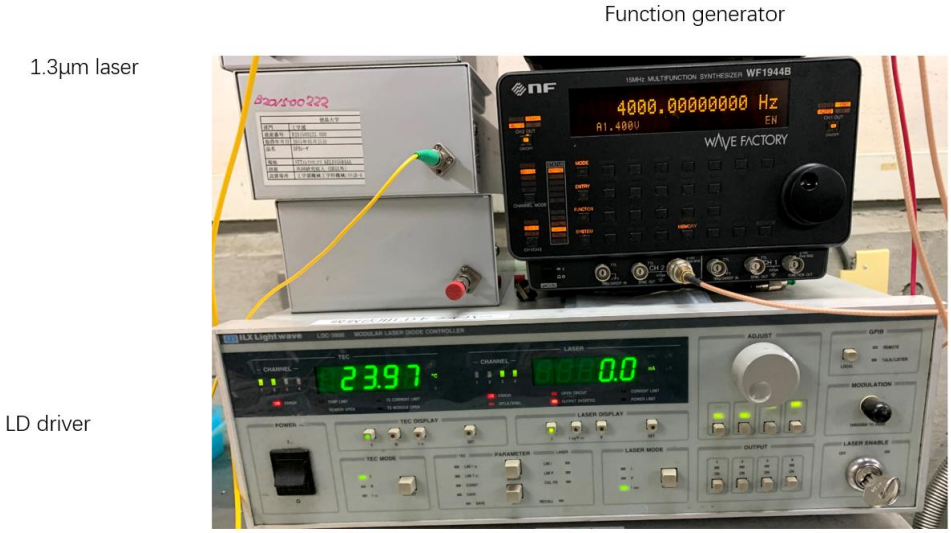

Fig. 3.10 DFB laser system

3.6 Low-temperature coal pyrolysis process measurement using TDLAS

Experimental setup is shown in Fig. 3.5 and Fig. 3.6. Basically, the setup is like hydrocarbon measurement, the difference is hydrocarbon cylinder was replaced by A heating chamber that also connects to another nitrogen cylinder. Coal powder was placed inside heating chamber. Gas pipes and absorbing cell were wrapped with heating tapes and heat isolation material for temperature conservation. Temperature of absorbing cell and heating chamber can be adjusted separately. Heating chamber was heated from 100℃ to 350℃ to investigate how temperature would affect volatilization process while temperature of other parts was kept the same. Nitrogen flow was set to 50mL/min when measuring and stopped when heating chamber was heated to various temperatures.

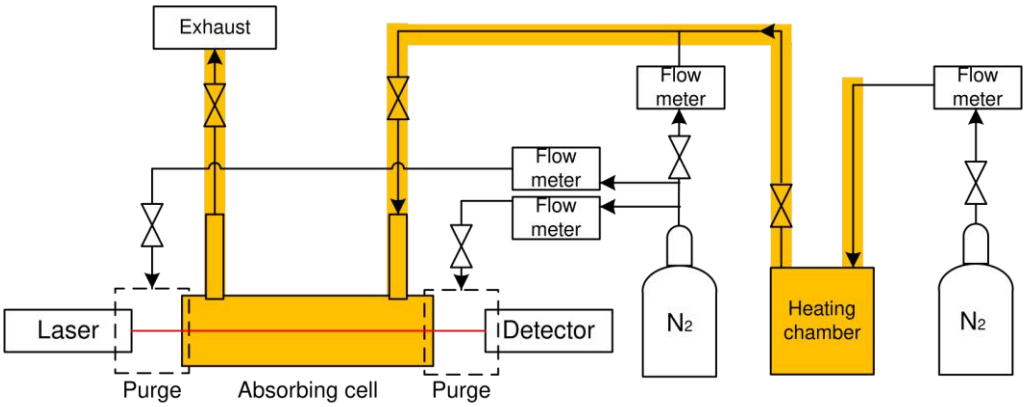

Fig. 3.11 Coal pyrolysis measurement setup

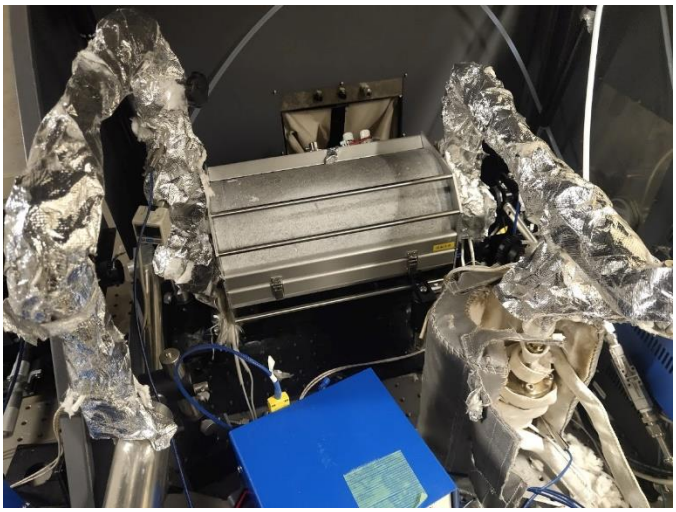

Fig. 3.12 setup photo

4 Results and discussion

4.1 Laser performance

Common spectroscopic databases for hydrocarbon molecules include HITRAN [39], HITEMP [52], PNNL [53] and others (cf. Table 4 in [54]). These databases provide line parameters or measured cross sections for common hydrocarbon molecules. Detailed line parameters for methane and ethylene were included in the HITRAN database. For other molecules mentioned in this work, only cross section information was available. Previous reports for all the fifteen hydrocarbon measurement on the 3μm region were summarized in Table 3 [53], [55]–[60]. As can be seen from the table, most of the molecules lack accurate models in the 3μm. The measured cross sections also have different measurement conditions. So, it is difficult to make a direct comparison between measured spectra and modeled spectra for each species. For sensitivity estimation, the 'per point' minimum detectable absorption (MDA_{pp}) was calculated.

Table 3 List of hydrocarbon spectra in the 3μm region reported by other researchers

Species	Data Type	Resolution (cm^{-1})	Laser approach	Reference
Methane (CH_4)	Line parameters	10^{-7}-10^{-6}	DFG	[55]
Ethene (C_2H_4)	Line parameters	0.02	FTIR	[56]
Ethane (C_2H_6)	Cross sections	0.004	FTIR	[57]
Propene (C_3H_6)	Cross sections	0.112	FTIR	[53]
Propane (C_3H_8)	Cross sections	0.015	FTIR	[58]
n-Butane (C_4H_{10})	Cross sections	0.112	FTIR	[53]
n-Pentane (C_5H_{12})	Cross sections	0.1	FTIR	[59]
n-Hexane (C_6H_{14})	Cross sections	0.112	FTIR	[53]
Methylcyclohexane (C_7H_{14})	Cross sections	/		Not reported
n-Heptane (C_7H_{16})	Cross sections	0.1	FTIR	[59]
Diisobutylene (C_8H_{16})	Cross sections	/		Not reported
Isooctane (C_8H_{18})	Cross sections	0.1	FTIR	[59]
Benzene (C_6H_6)	Cross sections	0.112	FTIR	[60]
Toluene (C_7H_8)	Cross sections	0.1	FTIR	[59]

m-Xylene (C_8H_{10})	Cross sections	0.1	FTIR	[59]

The minimum detectable absorption (MDA) is a value cited by many researchers to evaluate the sensitivity performance of the system. The MDA_{pp} was chosen since this definition is independent of scan characteristics and can be used to compare with other instruments. The MDA_{pp} can be expressed as:

$$MDA_{pp} = \left(\frac{\Delta P}{P}\right)_n \frac{1}{\sqrt{BW}} \qquad (4.1)$$

where $\frac{\Delta P}{P}$ represents the limiting noise level of a measurement normalized by the total power, and BW is the sampling bandwidth.

To determine the noise level, a comparison between one measured nitrogen spectrum and a polynomial fit to the data was made. The result was shown in Fig. 4.1. The mean square error of MSE=0.125% was obtained by calculating the square deviation of each point. This value was used as $\frac{\Delta P}{P}$ and a sampling rate of 6kHz yields to a value of $MDA_{pp}=2.29\times10^{-5}Hz^{-1/2}$. Due to the high sampling rate, the minimum detectable absorption of the proposed system is competitive compare to other broadband spectroscopic techniques (cf. Table 5 in [54]).

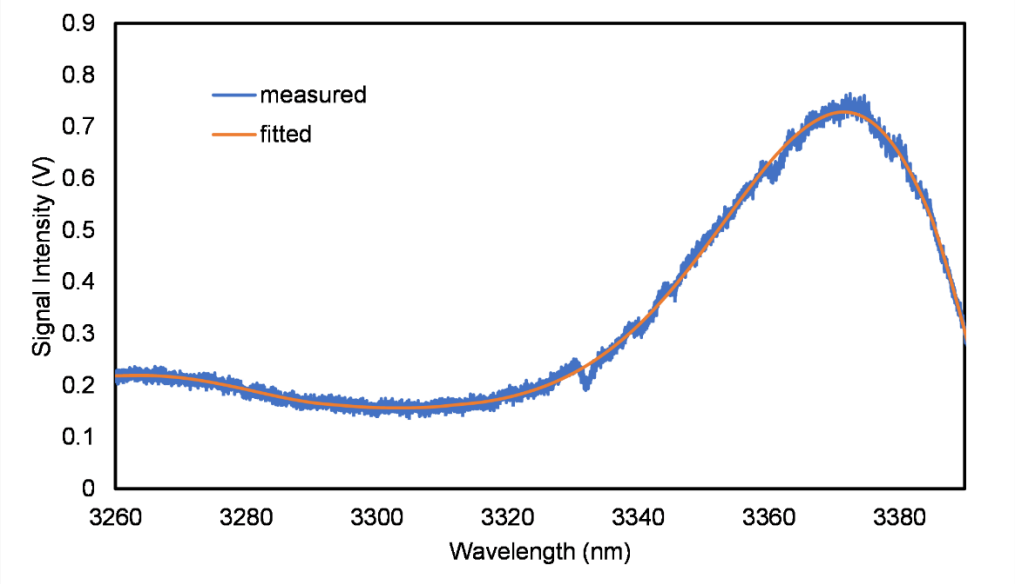

Fig. 4.1 Measured spectrum and polynomial fit to the data

As listed in Table 3, the FTIR is the mainstreaming approach for hydrocarbon measurement. Different FTIR spectrometers have trade-off between sensitivity, path length, spectral resolution and calibration. The proposed laser system also has the same trade-off. There are some merits and demerits that need to be mentioned. The proposed system is a portable device system with light

weight and relatively cheap components. Although its sensitivity and resolution are no match for high-end instruments, a relatively good performance can be achieved when compared to other portable FTIR devices. Another merit over the FTIR is the calibration free feature (cf. Fig. 6.7 in [38]). This feature ensures the proposed system to be unaffected by dust or small vibrations. The demerit of the proposed system is FTIR method can cover a broader scanning range and reduce the complexity of mixture analysis.

4.2 Single and mixture hydrocarbon measurement result

Hydrocarbons consist a large group of organic compounds. It would go beyond the scope of this paper to conduct measurement of all the possible hydrocarbon gases and their numerous possible combinations. The spectra of chosen hydrocarbons afore mentioned will be presented with each molecule's number of carbon atoms ranging from one to ten. Concentration and temperature dependence measurement were carried out for quantitative analysis. Measurement of several chosen mixtures were also conducted for validation and analysis and their results will be presented here too.

4.2.1 single species measurement

Because of the different composition of atoms and molecular structure, absorption of hydrocarbons is caused by different vibrational modes and thus makes each molecule has a unique absorption pattern, which can be used to identify its kind. Although the number of carbon atoms will cause a bigger change in absorption spectra comparing to the difference in molecular structures, hydrocarbons that belong to the same group also tend to have similar absorption shapes, especially when the number of carbon atoms was higher. Hence, we loosely divided the results of single species measurements into several parts considering both factors.

Figure 4.2 and Fig. 4.3 displayed the measurement results of CH_4 and C_2H_6. They have very few carbon atoms which means the structures are relatively simple, and the absorption lines are sharper compared to heavier molecules. The 3280.5nm and 3336.4nm lines of CH_4 and C_2H_6 respectively were selected for quantitative analysis. The lines chosen for these two positions were to stay in the relatively shorter wavelength among the whole scanning range where heavier aliphatic compounds tend to have absorption in longer wavelength regions. The R^2 value is a good indicator of the uncertainty in the experiments. The R^2 value of CH_4 concentration dependence result was smaller which may be caused by the undistributed laser signal intensity where the signal

in shorter wavelength was weaker, thus would cause more fluctuation in absorbance. Absorption spectra of CH_4 were measured at 5 discrete temperatures between 20℃ and 450℃ and the calibration line was also plotted and was shown in Fig. 5(c) using the same absorption line. The results showed that the spectra are dependent on temperature.

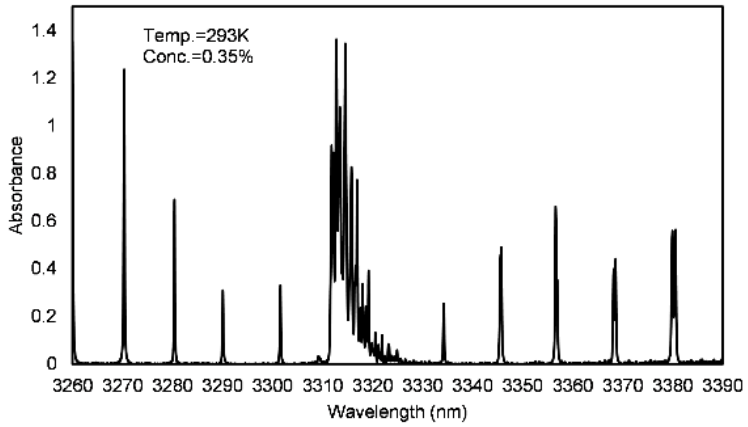

(a) Absorption spectrum of CH_4

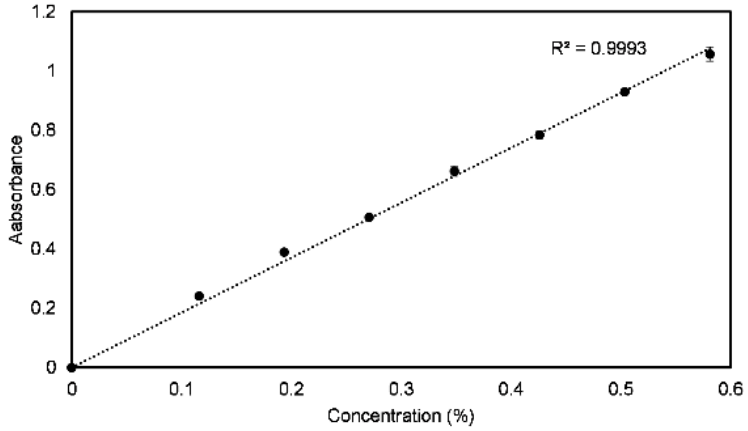

(b) Concentration dependence of absorbance

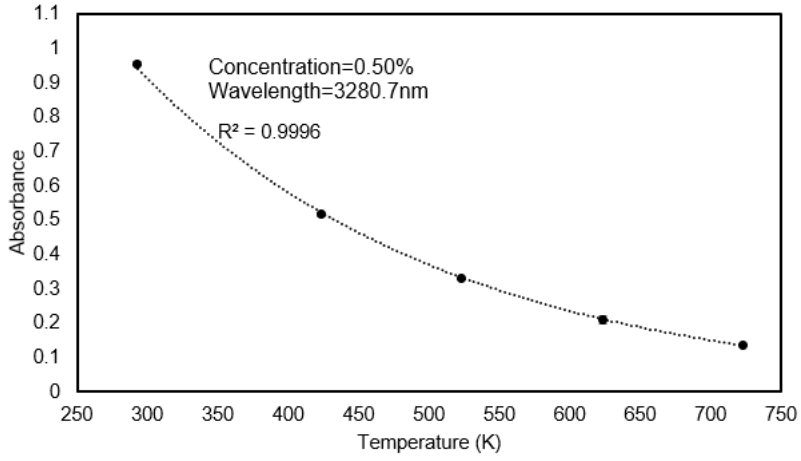

(c) Temperature dependence of absorbance

Fig. 4.2 Measurement results of CH_4

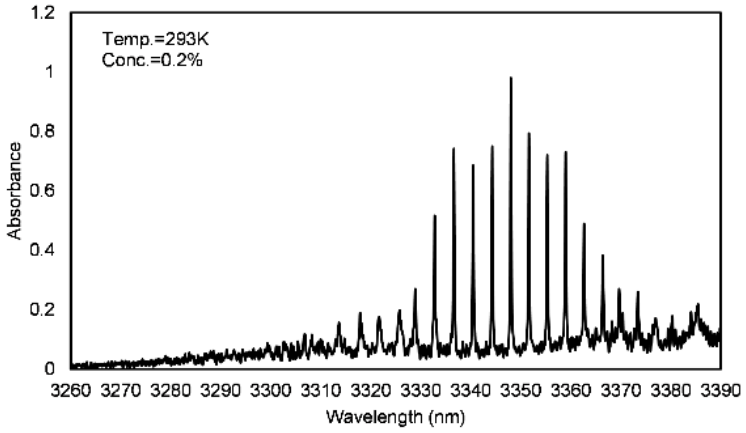

(a) Absorption spectrum of C_2H_6

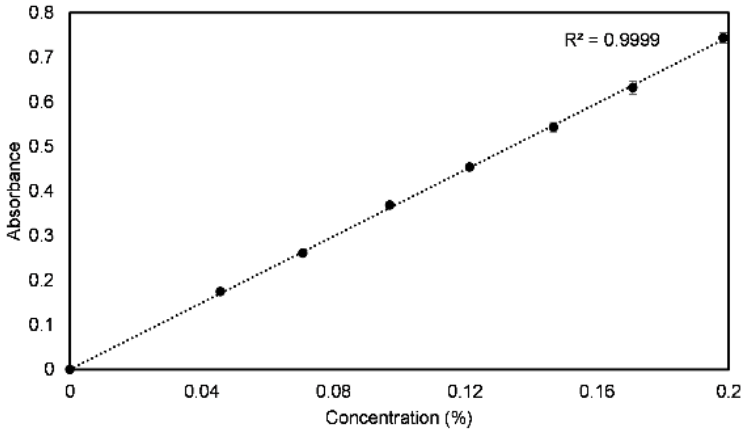

(b) Concentration dependence of absorbance

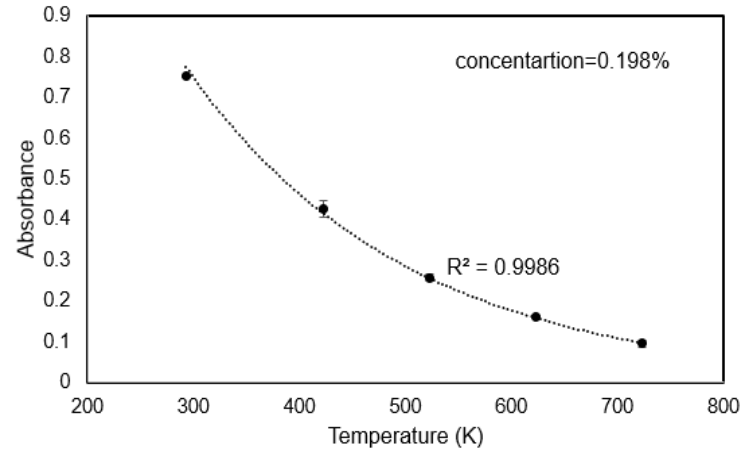

(c) Temperature dependence of absorbance

Fig. 4.3 Measurement result of C_2H_6

The results of C_2H_4 and C_3H_6 were depicted in Fig. 4.4 and Fig. 4.5. Unlike CH_4 and C_2H_6, these two straight alkenes have more evenly distributed absorption in the scanning wavelength. The 3346nm and 3384.9nm peaks were chosen for plotting calibration lines. The R^2 value of the C_3H_6 result was smaller which was due to the chosen peak was at the edge of the whole spectrum where the slope of signal intensity was large and therefore was easier to fluctuate.

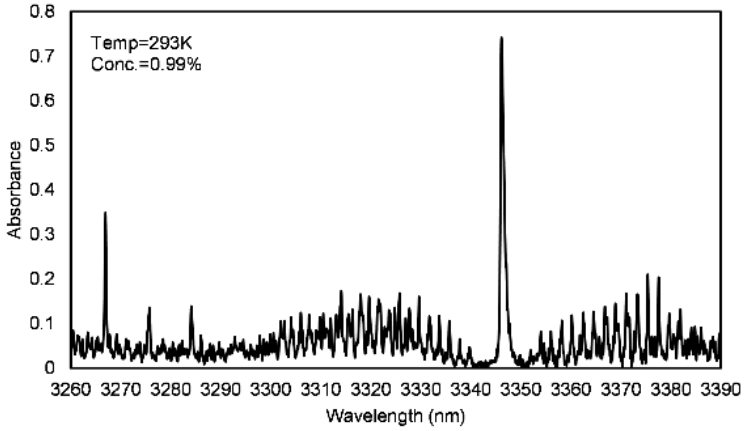

(a) Absorption spectrum of C_2H_4

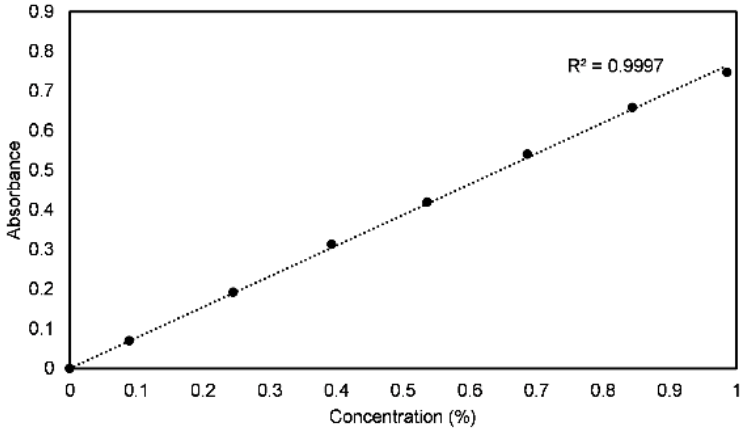

(b) Concentration dependence of absorbance

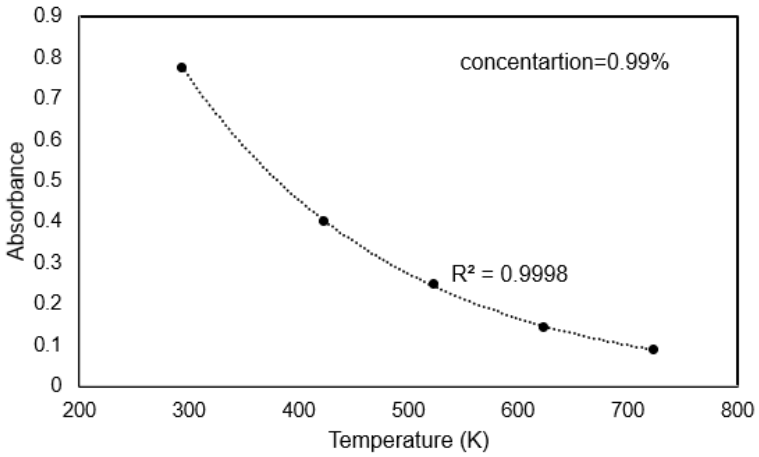

(c) Temperature dependence of absorbance

Fig. 4.4. Measurement result of C_2H_4

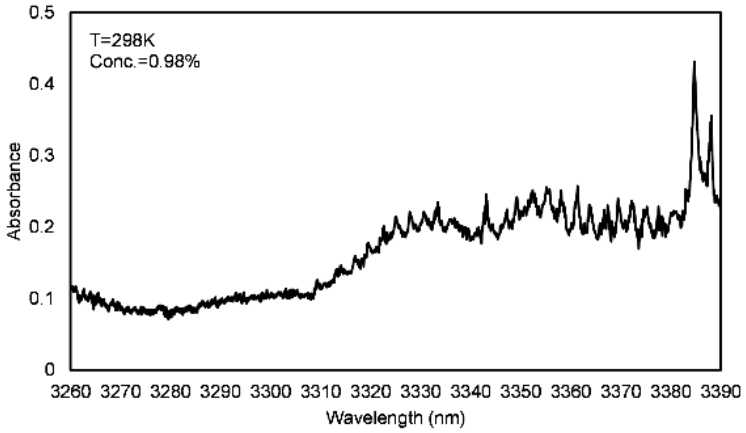

(a) Absorption spectrum of C_3H_6

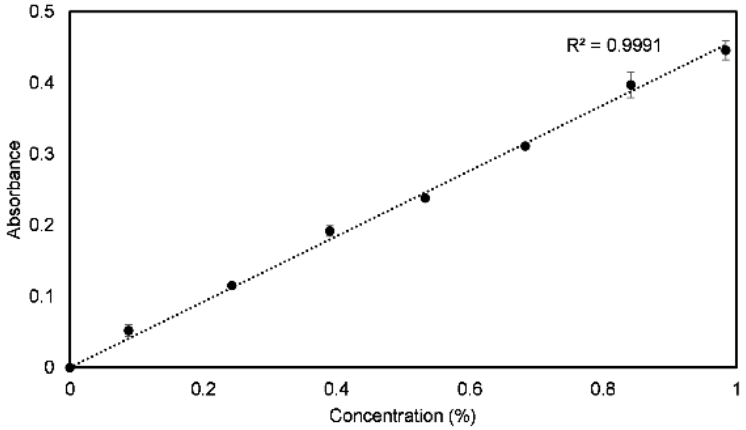

(b) Concentration dependence of absorbance

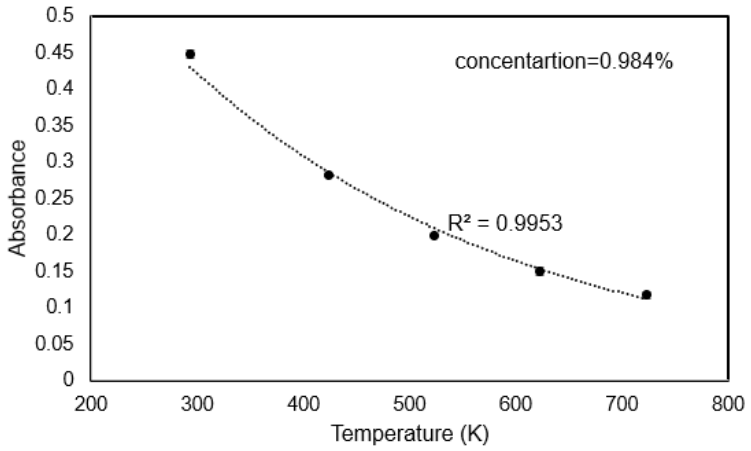

(c) Temperature dependence of absorbance

Fig. 4.5 Measurement result of C_3H_6

Figure 4.6 and Fig. 4.7 presented the results of C_3H_8 and C_4H_{10}. They share similar absorption spectra, which is the result of the CH_3 asymmetric vibrational mode (for C_4H_{10}, the CH_2 asymmetric mode also has an impact, probably due to the equal number of CH_2 and CH_3 groups [61]). The peak positions chosen for C_3H_8 and C_4H_{10} were 3369.8nm and 3370.4nm, respectively. The R^2 values of these two species were the biggest which are identical to the strong signal intensity in this area.

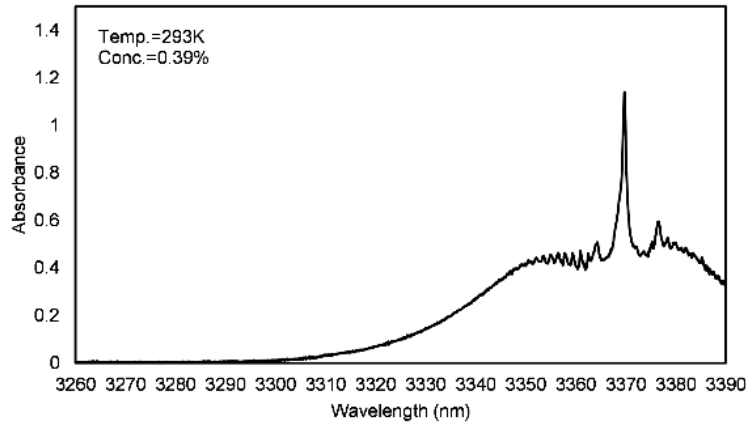

(a) Absorption spectrum of C_3H_8

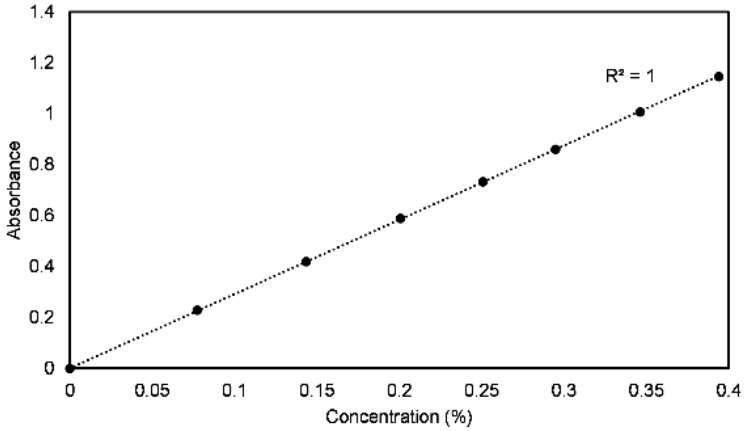

(b) Concentration dependence of absorbance

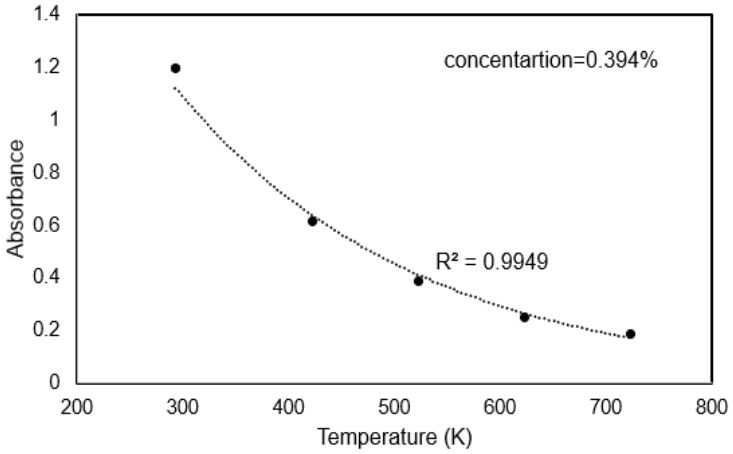

(c) Temperature dependence of absorbance

Fig. 4.6. Measurement result of C_3H_8

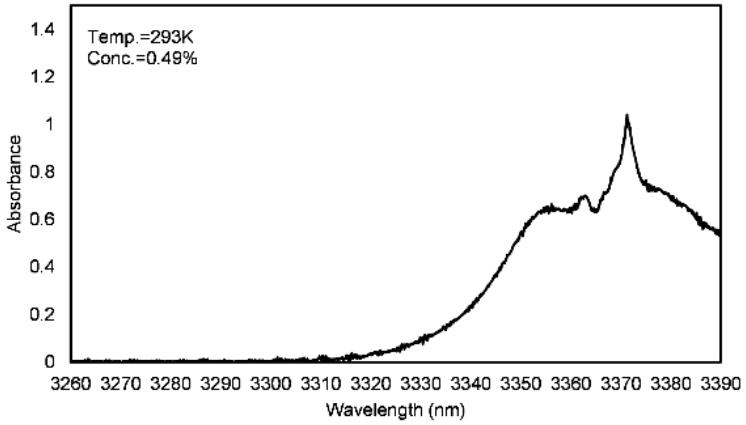

(a) Absorption spectrum of C_4H_{10}

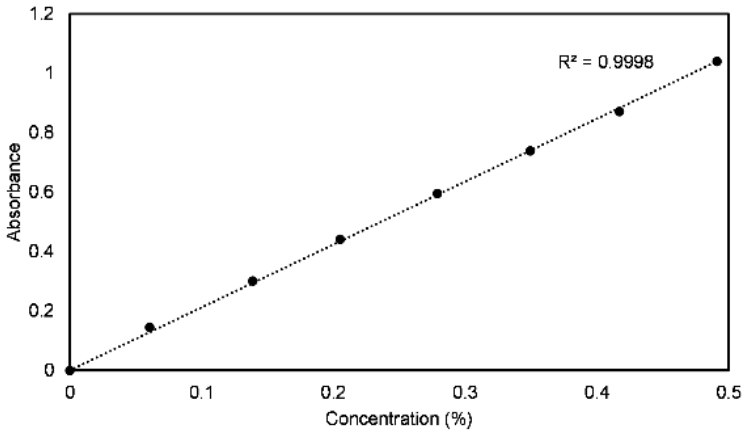

(b) Concentration dependence of absorbance

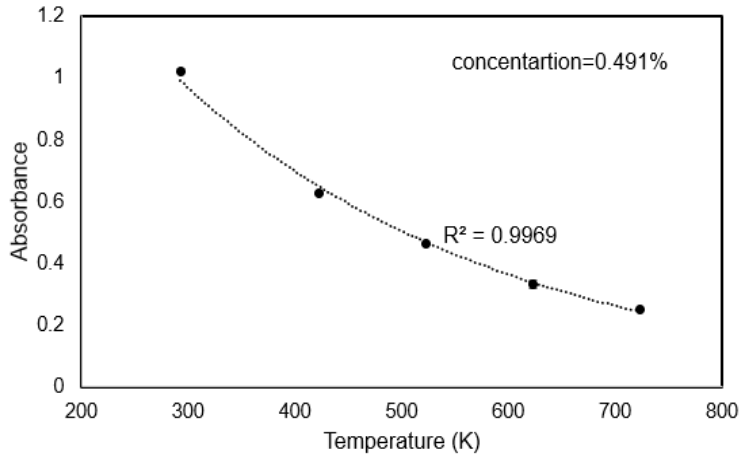

(c) Temperature dependence of absorbance

Fig. 4.7 Measurement result of C_4H_{10}

Figure 4.8-4.10 depicted the results of C_5H_{12}, C_6H_{14}, C_7H_{14}, and C_7H_{16}. These molecules are all aliphatic hydrocarbons with more than 5 carbon atoms. From the spectra, we can no longer find isolated narrow absorption peaks but only barely distinguishable peaks among wide absorption in wavelength over 3340nm due to the complex structure of polyatomic molecules.

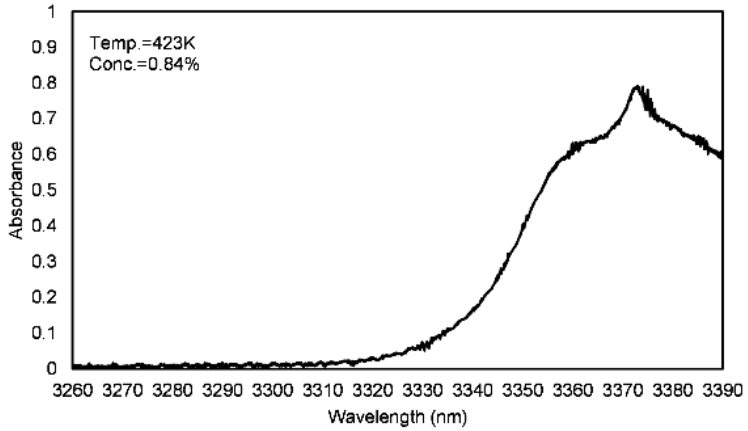

(a) Absorption spectrum of C_5H_{12}

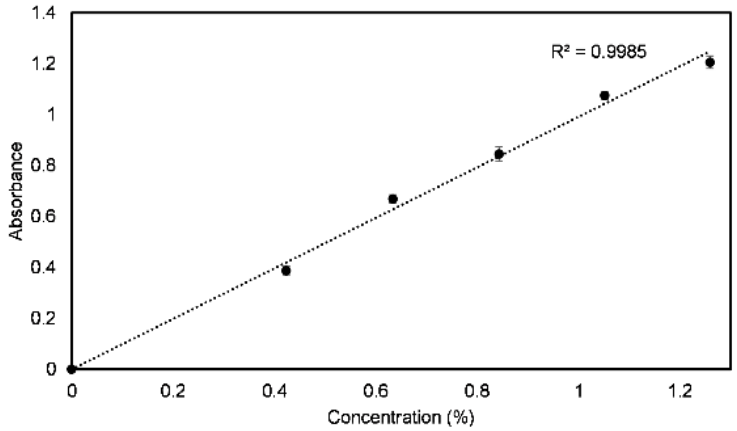

(b) Concentration dependence of absorbance

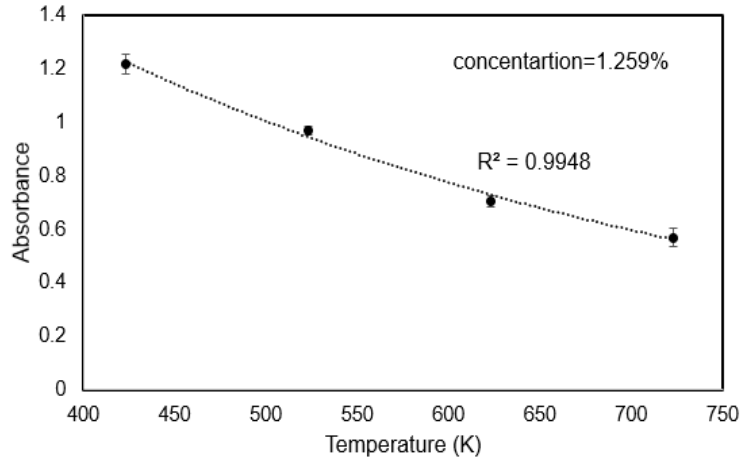

(c) Temperature dependence of absorbance

Fig. 4.8 Measurement result of C_5H_{12}

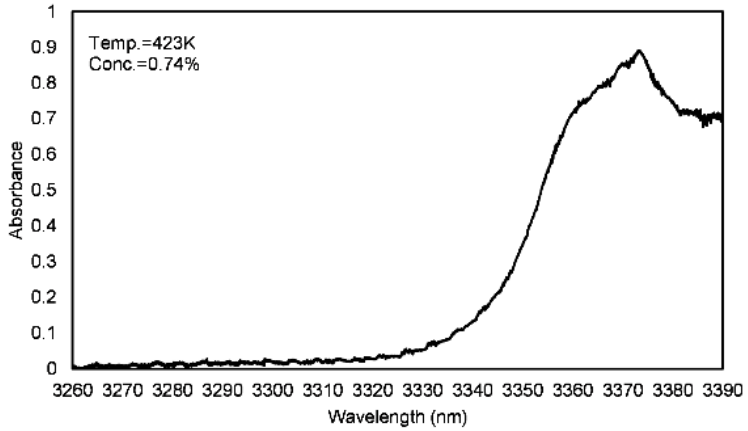

(a) Absorption spectrum of C_6H_{14}

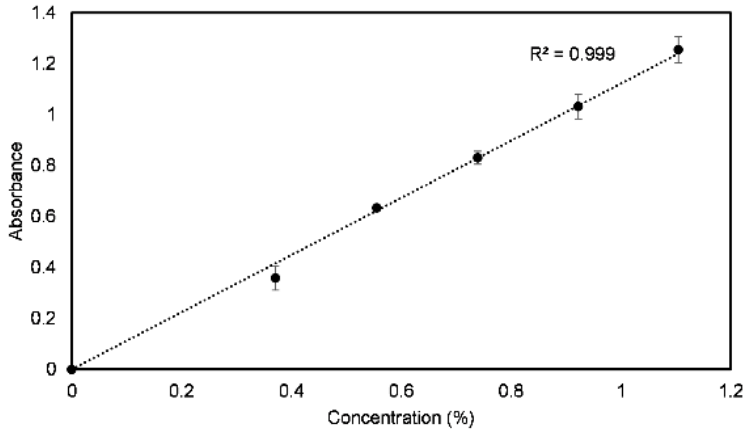

(b) Concentration dependence of absorbance

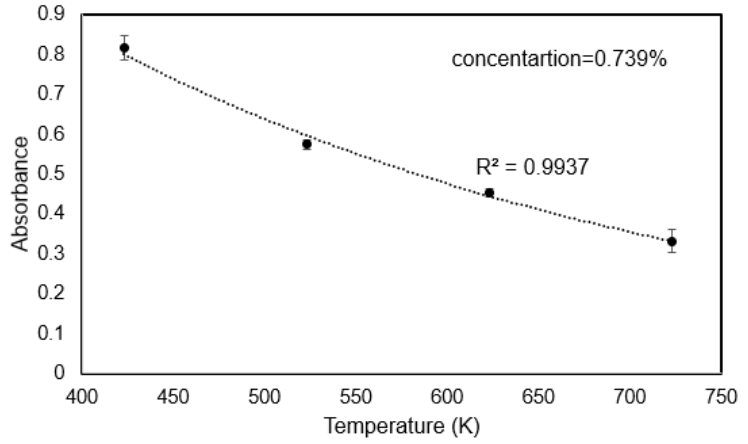

(c) Temperature dependence of absorbance

Fig. 4.9 Measurement result of C_6H_{14}

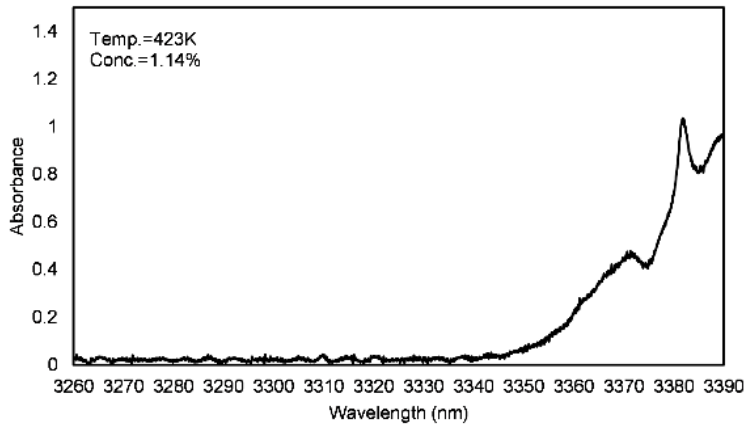

(a) Absorption spectrum of C_7H_{14}

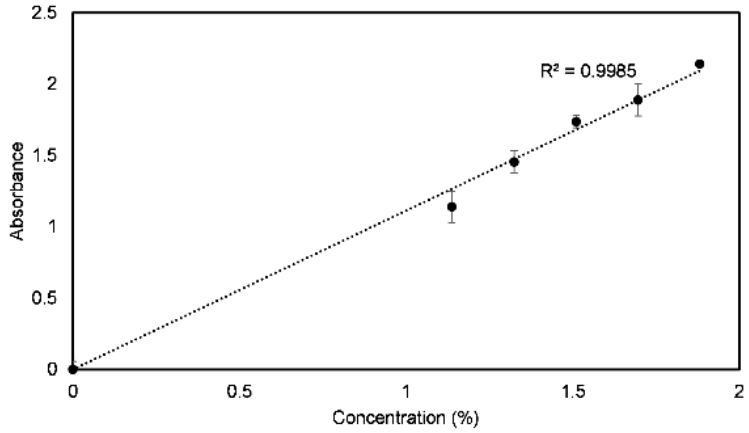

(b) Concentration dependence of absorbance

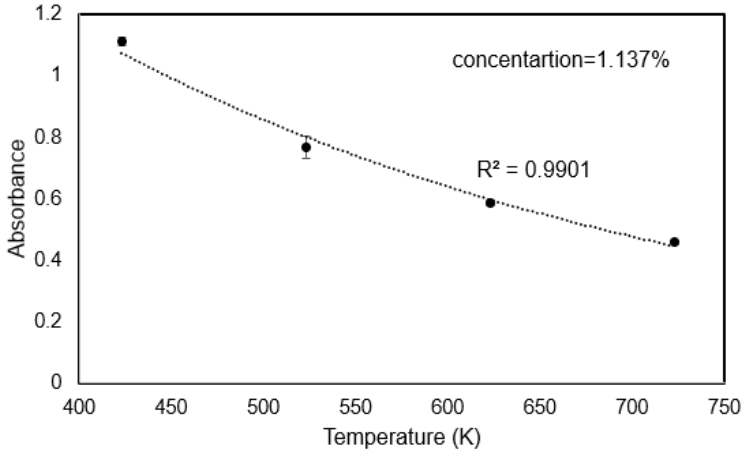

(c) Temperature dependence of absorbance

Fig. 4.10 Measurement result of C_7H_{14}

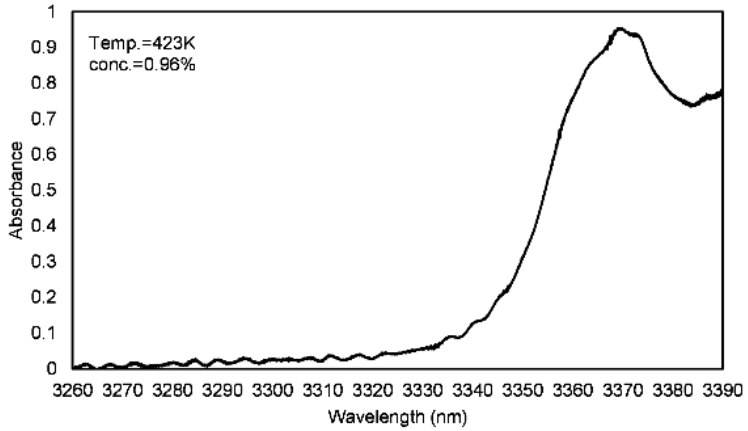

(a) Absorption spectrum of C_7H_{16}

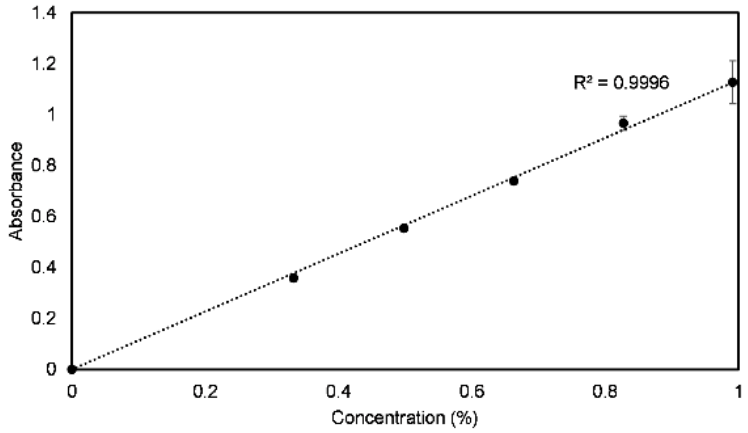

(b) Concentration dependence of absorbance

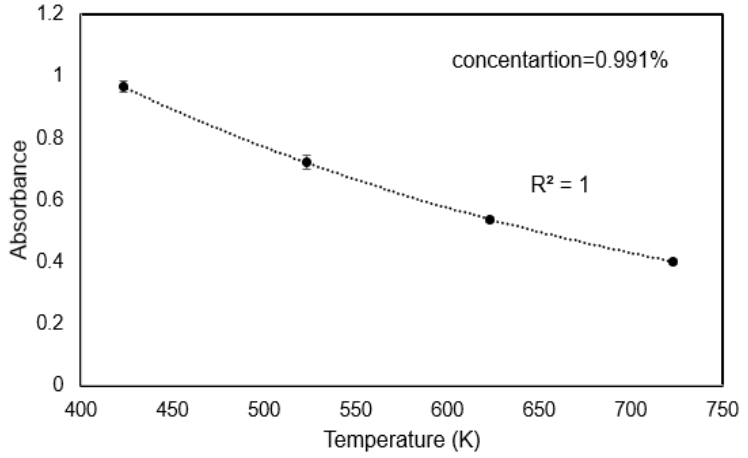

(c) Temperature dependence of absorbance

Fig. 4.11 Measurement result of C_7H_{16}

Fig. 4.11 and Fig. 4.12 provided the result of C_8H_{16} and C_8H_{18}, both of which only have blunted curves and indicates the limitation of the measurement system.

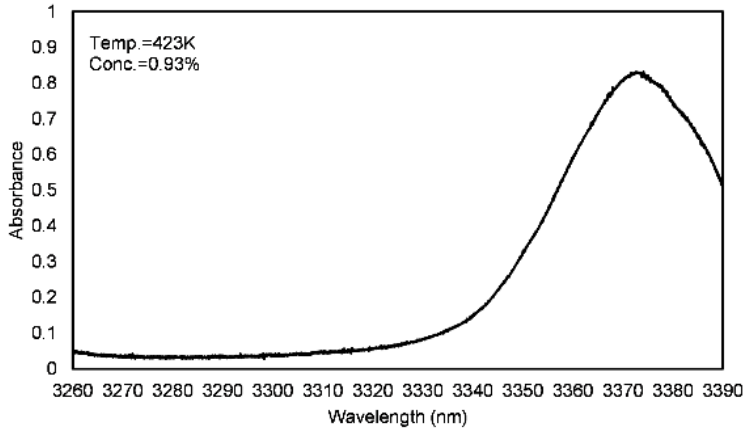

(a) Absorption spectrum of C_8H_{16}

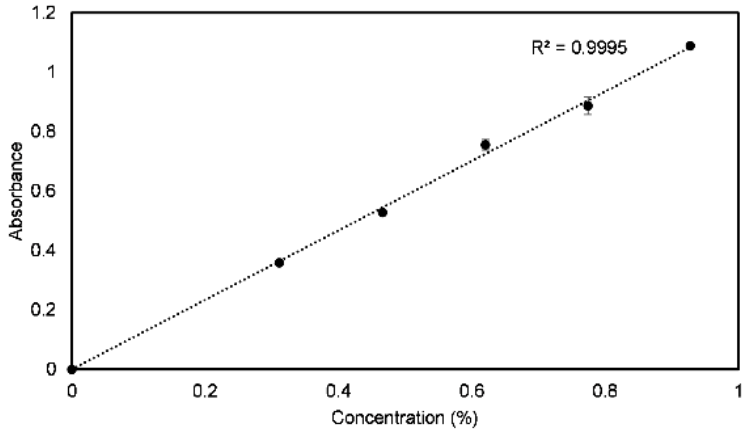

(b) Concentration dependence of absorbance

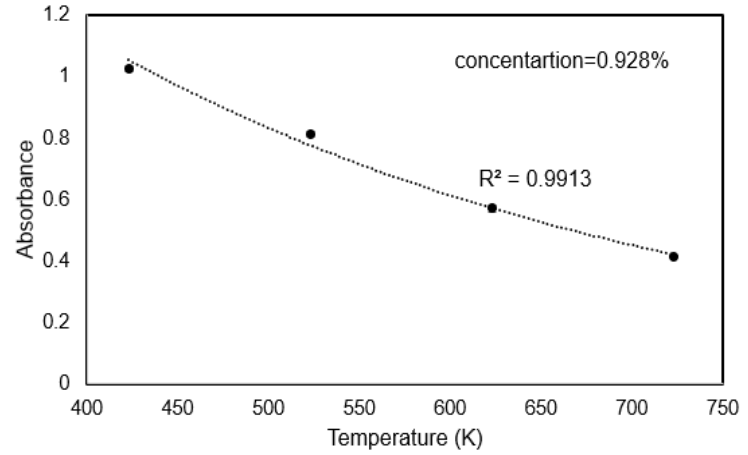

Fig. 4.12 Measurement result of C_8H_{16}

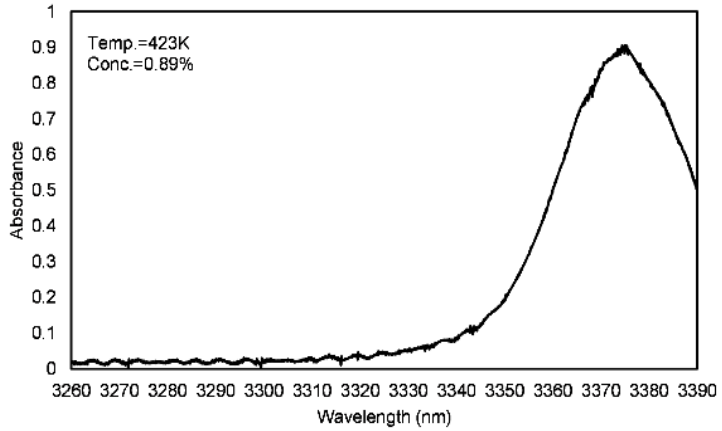

(a) Absorption spectrum of C_8H_{18}

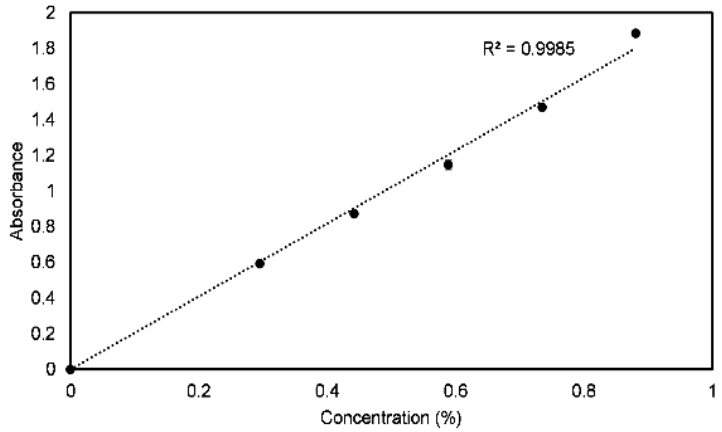

(b) Concentration dependence of absorbance

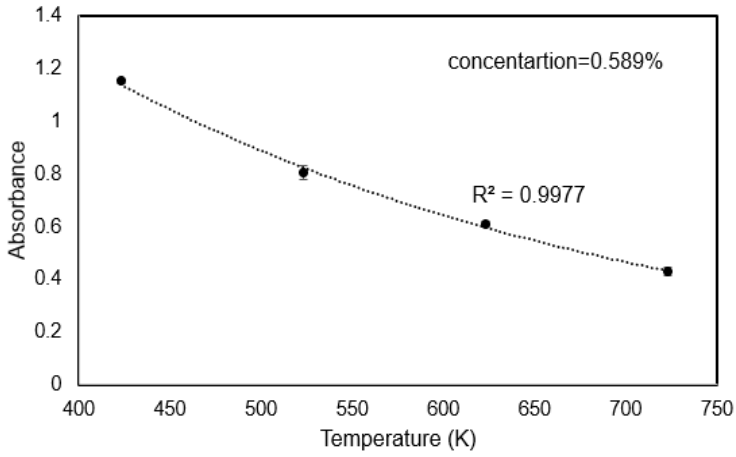

(c) Temperature dependence of absorbance

Fig. 16. Measurement result of C_8H_{18}

Figure 4.13-4.15 illustrates the results of C_6H_6, C_7H_8, C_8H_{10}. These three molecules belong to the aromatic group. Although their absorption spectra are also the result of C-H stretching, unlike the alkyl C-H stretching, the aromatic stretching is in a shorter wavelength region (below 3320nm), while the higher absorption area of heavier aliphatic compounds is over 3340nm. Like other molecules with a greater number of carbon atoms, these aromatics also do not have very sharp peaks. The uncertainty of these vapor phase molecule concentration dependence of absorbance results was larger than light molecules due to the different experimental setup.

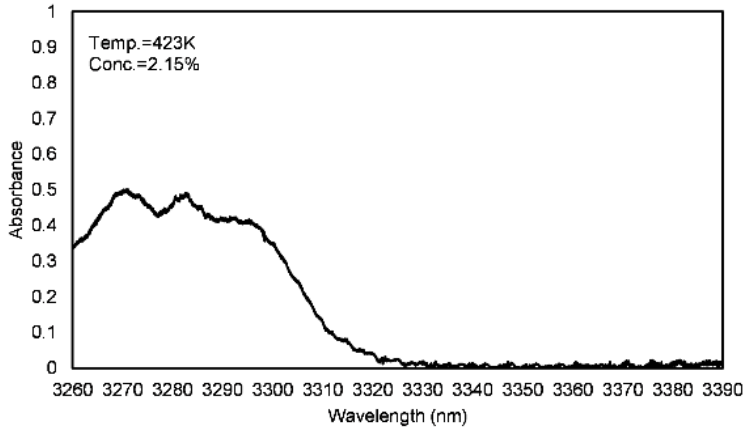

(a) Absorption spectrum of C_6H_6

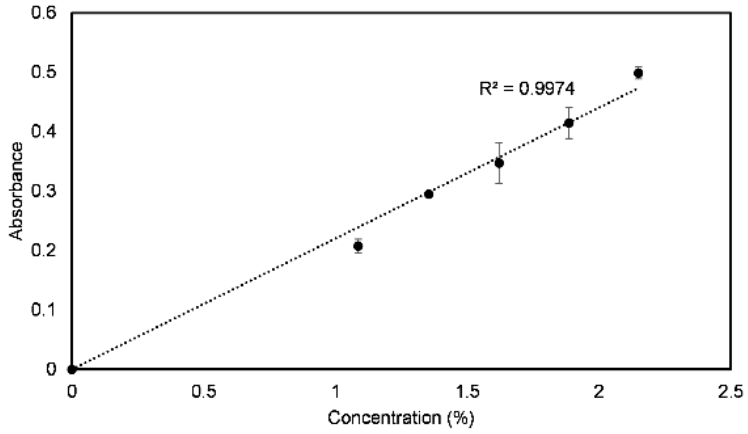

(b) Concentration dependence of absorbance

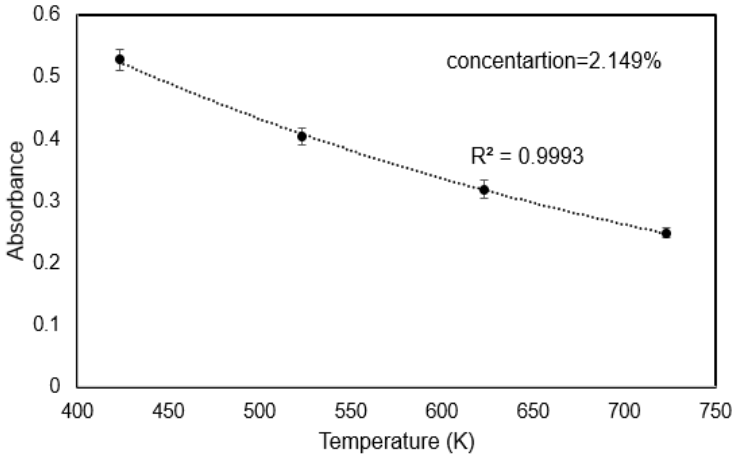

(c) Temperature dependence of absorbance

Fig. 4.13 Measurement result of C_6H_6

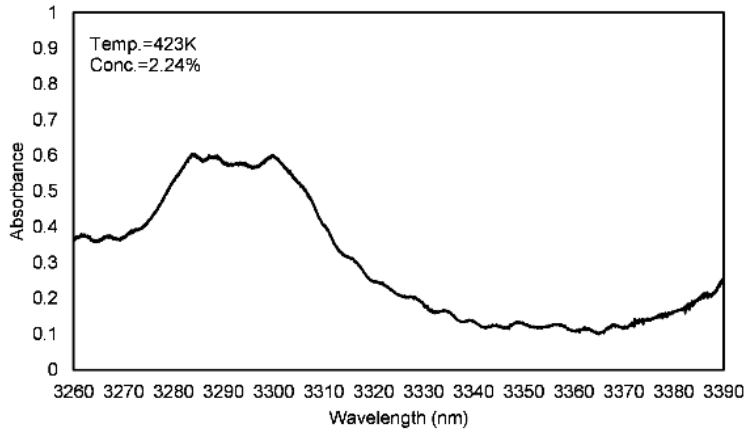

(a) Absorption spectrum of C_7H_8

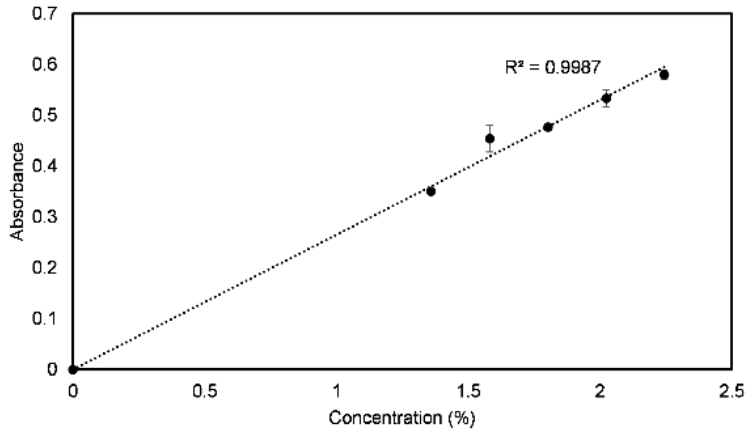

(b) Concentration dependence of absorbance

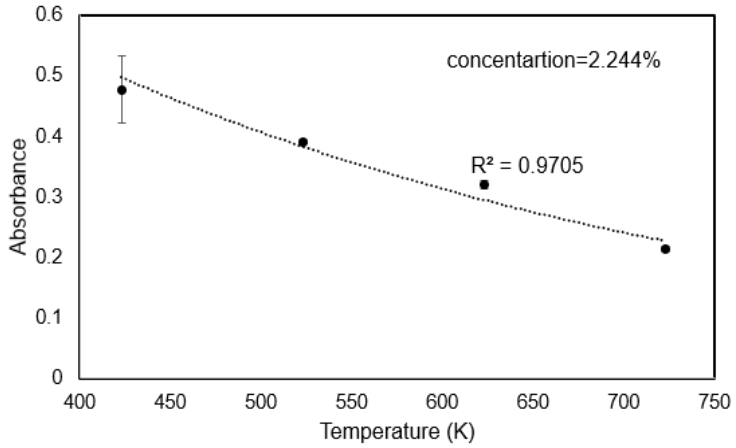

(c) Temperature dependence of absorbance

Fig. 4.14 Measurement result of C_7H_8

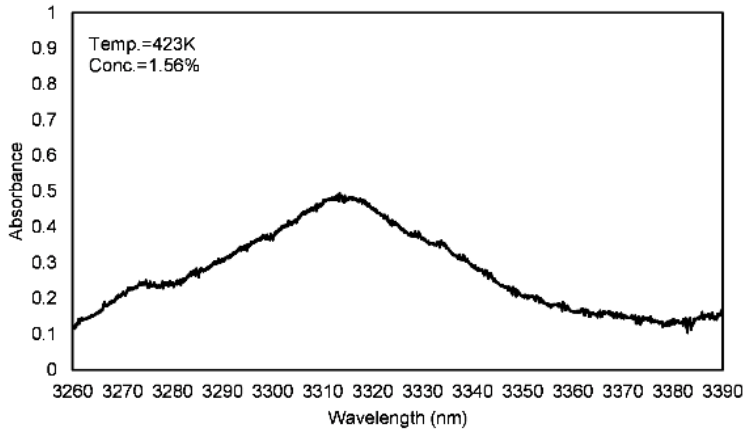

(a) Absorption spectrum of C_8H_{10}

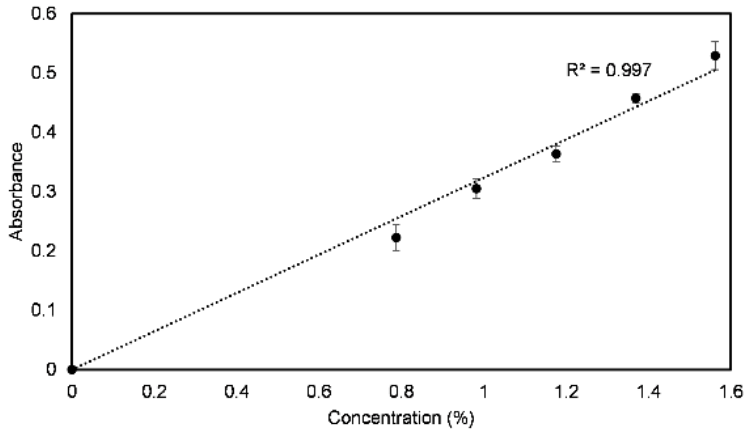

(b) Concentration dependence of absorbance

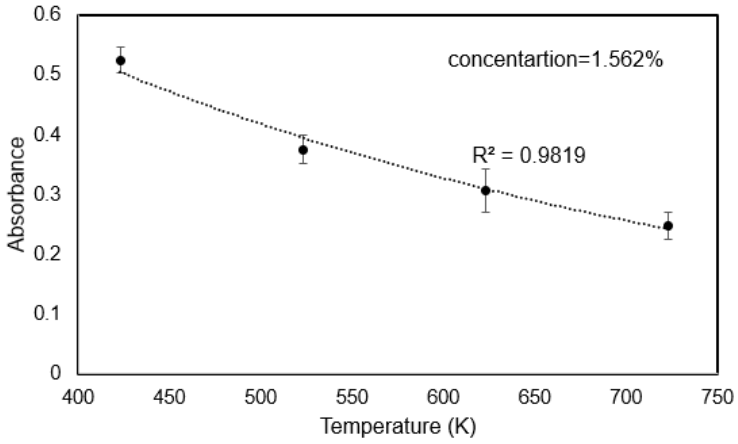

(c) Temperature dependence of absorbance

Fig. 4.15 Measurement result of C_8H_{10}

To further analysis the concentration dependence of absorbance, for each species, five different wavelengths were picked to calculate the concentration dependence on absorbance. The selected wavelengths were to keep a relatively constant gap, and the absorption peaks were picked over an integer wavelength if peaks exist. The selected wavelengths, minimum and maximum R^2 values for the concentration dependence results of each species were summarized in Table 4.

Table 4 Selected wavelength and R^2 values for single species

Species	Selected Wavelength (nm)	Minimum R^2	Maximum R^2
CH_4	3280.7, 3313.7, 3334.4, 3356.8, 3379.9	0.9991	0.9999
C_2H_4	3267.1, 3284.6, 3346.2, 3375.5, 3314.7	0.9994	0.9997
C_2H_6	3328.9, 3336.8, 3348.1, 3359.3, 3373.4	0.9994	0.9999
C_3H_6	3310.0, 3330.7, 3343.1, 3361.3, 3384.7	0.9979	0.9991
C_3H_8	3330.0, 3345.0, 3369.7, 3376.6, 3385.0	0.9991	0.9999
C_4H_{10}	3330.0, 3345.0, 3362.4, 3371.2, 3385.0	0.9998	0.9999
C_5H_{12}	3340.0, 3350.0, 3360.0, 3372.4, 3385.0	0.9982	0.9986
C_6H_{14}	3340.0, 3350.0, 3360.0, 3373.3, 3385.0	0.9990	0.9992
C_7H_{14}	3350.0, 3360.0, 3370.0, 3381.6, 3385.0	0.9969	0.9986
C_7H_{16}	3340.0, 3350.0, 3360.0, 3370.0, 3380.0	0.9994	0.9996
C_8H_{16}	3340.0, 3350.0, 3360.0, 3370.0, 3385.0	0.9987	0.9996
C_8H_{18}	3340.0 ,3350.0, 3360.0, 3370.0, 3385.0	0.9978	0.9992
C_6H_6	3265.0, 3275.0, 3285.0, 3295.0, 3305.0	0.9963	0.9978

C_7H_8	3265.0, 3275.0, 3285.0, 3295.0, 3305.0	0.9985	0.9990
C_8H_{10}	3275.0, 3290.0, 3305.0, 3320.0, 3335.0	0.9963	0.9976

The overall R^2 values were bigger than 0.996, indicating good linear fitting results with small variance. The single species measurement results proved the system can measure hydrocarbons covering different molecular classes. The measured spectra of different hydrocarbons showed that the system has the potential to separately detect hydrocarbons with up to eight carbon atoms.

Naphthalene is in solid state under room temperature, so it is impossible to directly inject naphthalene into the absorbing cell. To achieve the measurement of these solid hydrocarbons, we use the hexane as the solvent, and dissolve naphthalene into hexane. The mixture of naphthalene and hexane was measured and compared with pure hexane results. By subtracting the absorption spectra, the spectra of naphthalene were obtained.

The measurement results were displayed in Fig. 4.16. Like other aromatic hydrocarbons, the absorption of naphthalene appears near the wavelength smaller than 3300nm.

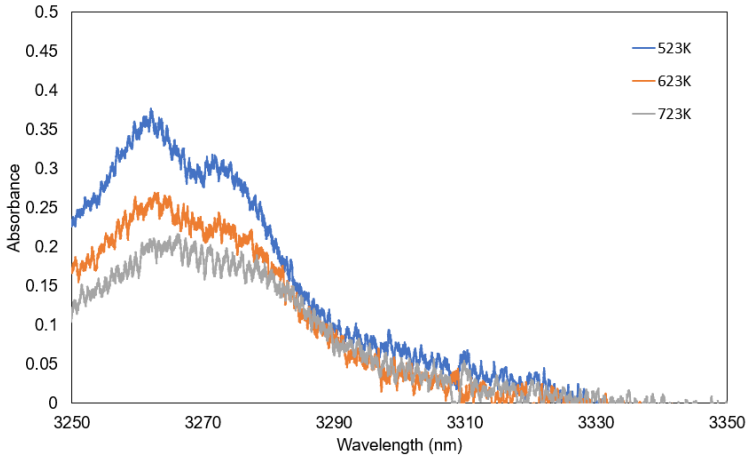

Fig. 4.15 Measurement result of C_8H_{10}

4.2.2 single species measurement using the ECD laser

The measurement of some heavy hydrocarbon molecules was also performed using a ECD laser working near the wavelength from 1670nm to 1685nm to compare the performance with the DFG laser.

The measurement results for C_8H_{16} were shown in Fig. 4.16.

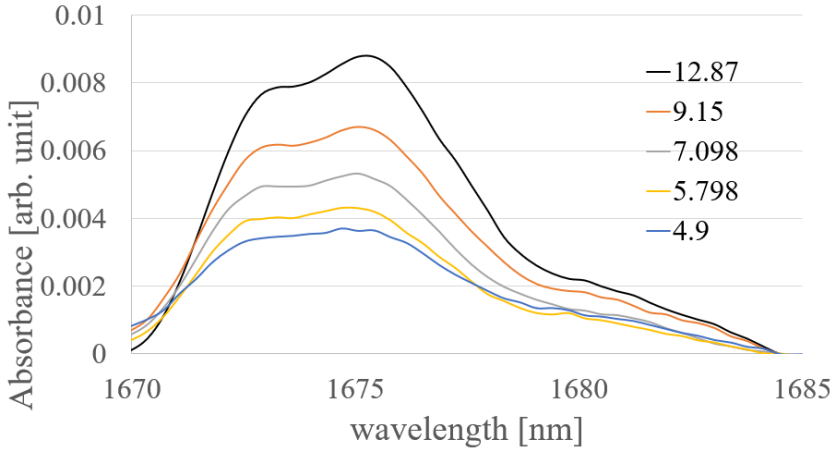

(a) absorption spectra under different concentrations

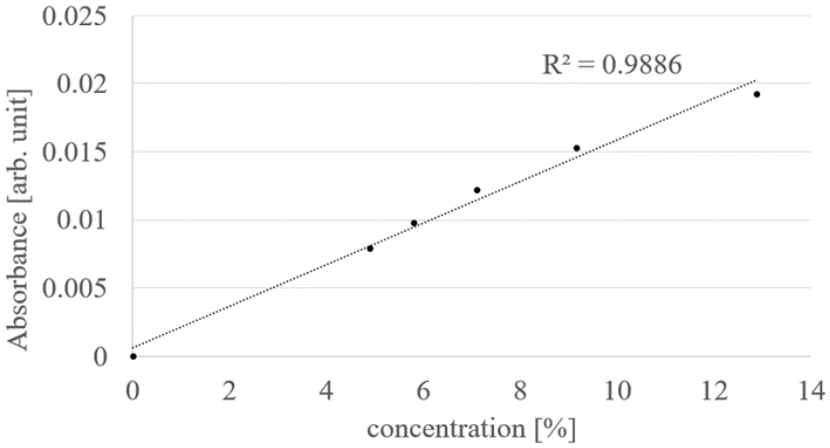

(b) Concentration dependence of absorbance

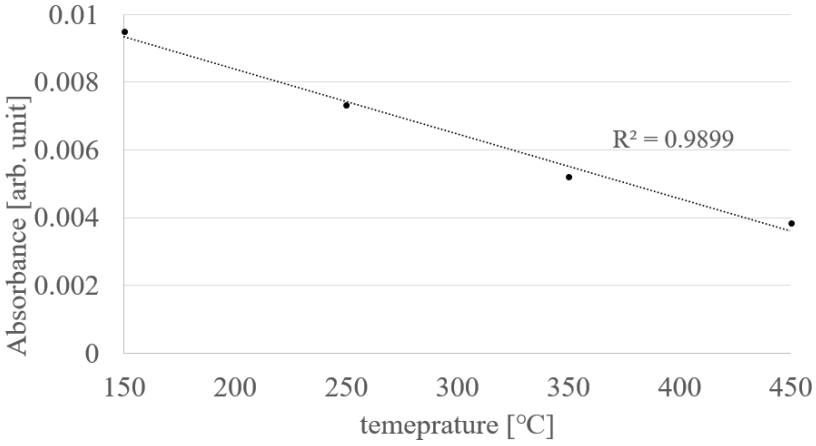

(c) Temperature dependence of absorbance

Fig. 4.16 Measurement result of C_8H_{16} using the ECD laser

As can be seen from the results, Even the concentrations of C_8H_{16} were much higher than the experiments performed using the DFG laser, much weaker absorption were observed. This is due to the fact that C-H bond in the 3μm was much stronger than in the 1.7μm. Hence the DFG laser is more sensitive in hydrocarbon detection and has better performance than the ECD laser.

4.2.3 signal to noise ratio and limit of detection

To determine the limit of detection for each species, we first need to calculate the average noise level. By measuring the blank signal using nitrogen, the residual between nitrogen signal was used to calculate the noise, as shown in Fig. 4.17.

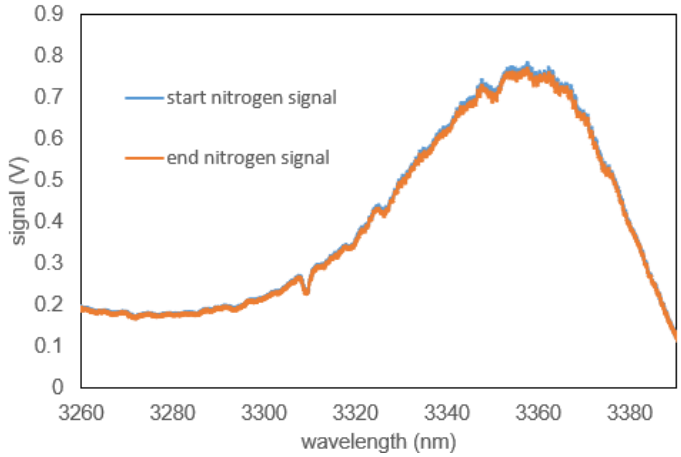

(a) blank spectra of nitrogen

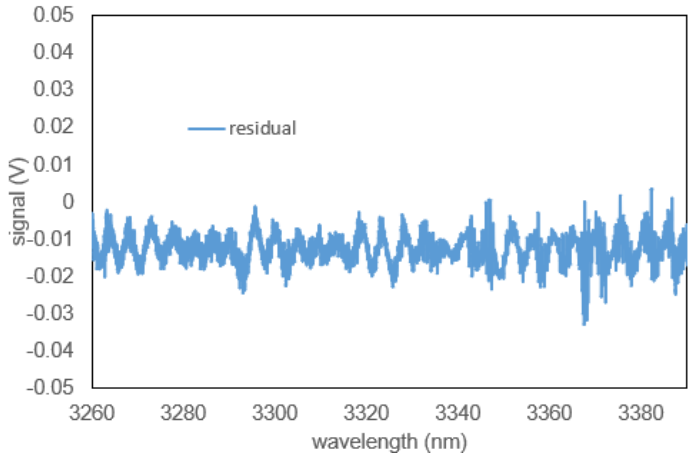

(b) residual between blank signals

Fig. 4.17 Blank measurement result

By performing eighteen experiments for five discrete temperatures ranging from 293K to 723K, an average root mean squares of 0.00624 was obtained and was taken as the noise level for the

measurement system. Then by using the peak absorbance of each molecule, the limit of detection for each molecule was also calculated. The results were shown in Table 5.

Table 5 Limit of detection for each molecule at different temperature

Species	293K	423K	523K	623K	723K
Methane (CH_4)	0.0017	0.0021	0.0027	0.0037	0.0075
Ethene (C_2H_4)	0.0092	0.0147	0.0222	0.0345	0.0675
Ethane (C_2H_6)	0.0014	0.0024	0.0033	0.0050	0.0130
Propene (C_3H_6)	0.0159	0.0209	0.0279	0.0331	0.0605
Propane (C_3H_8)	0.0024	0.0038	0.0058	0.0079	0.0154
n-Butane (C_4H_{10})	0.0035	0.0047	0.0060	0.0074	0.0138
n-Pentane (C_5H_{12})	/	0.0061	0.0070	0.0084	0.0147
n-Hexane (C_6H_{14})	/	0.0054	0.0071	0.0077	0.0129
Methylcyclohexane (C_7H_{14})	/	0.0061	0.0073	0.0077	0.0136
n-Heptane (C_7H_{16})	/	0.0060	0.0075	0.0086	0.0153
Diisobutylene (C_8H_{16})	/	0.0053	0.0063	0.0078	0.0156
Isooctane (C_8H_{18})	/	0.0030	0.0041	0.0048	0.0097
Benzene (C_6H_6)	/	0.0240	0.0287	0.0323	0.0595
Toluene (C_7H_8)	/	0.0274	0.0309	0.0338	0.0696
m-Xylene (C_8H_{10})	/	0.0173	0.0227	0.0235	0.0418

4.2.4 mixture measurement analysis using one wavelength

Since hydrocarbon mixtures rather than pure species exist in actual conditions, the performance of the system on mixture detection should also be evaluated. Although the proposed system has a wider scanning range compared to other tunable diode lasers, not all hydrocarbons have isolated absorption peaks, as discussed in the previous section. When multiple components co-exist in the mixture, it is usually difficult to find an absorption peak that is free from the interference of other species.

Here we use two methods to evaluate the mixture measurement results. The first method is to use one absorption peak for analysis and the second approach is to take advantage of the full spectra, by the combination usage of ICA and CLS method to achieve quantitative analysis.

For the mixtures with partially overlapped spectral bands, we chose isolated absorption peaks to check whether the results were different from single species detection. We applied the interferent correction method [62] to compare the results for fully overlapped mixtures. We considered one species as the analyte and the rest as interferent. The analyte and interferent both contribute to the absorbance at these peaks. Due to the additivity of the absorbance, the absorbance of the analyte was calculated using the following equation:

$$A_a = A_t - A_i \qquad (4.2)$$

Where the indices a, t, and i represent analyte, measured total, and interferent, respectively. The absorbance of interferent A_i was obtained using pure interferent data since the concentration of interferent is known. Then by using the reverse form of Beer-Lambert's law, concentration was calculated and compared with actual concentration.

The results of CH_4 and C_3H_8 mixture measurement were displayed in Fig. 4.18. As can be seen from Fig. 4.18(a), the spectra of CH_4 and C_3H_8 overlap with each other in the 3310-3390nm region while in the 3260-3310nm region CH_4 is isolated from interference. A strong absorption peak of C_3H_8 exists in 3369.8nm where the impact of CH_4 in this wavelength is minor due to its narrow peak shape. Two sets of experiments were carried out. In both experiments, one molecule serves as the analyte and the other serves as the interferent. The concentration of interferent remains constant while the concentration of analyte varies. The results were compared with the result of pure molecules obtained from single species measurement. By using the calibration line of pure single species, concentrations of analytes were calculated and compared with actual experiment concentration. (Assuming the absorbance in 3280.5nm and 3369.8nm represents the absorbance of CH_4 and C_3H_8, respectively). The x-axis and y-axis in Fig. 4.18(b) and Fig. 4.18(c) represented actual and calculated concentrations, respectively. The slopes of the least square fitting lines of the two figures were near 1, which indicated the interference between CH_4 and C_3H_8 was small. The variation and R^2 value of the CH_4 result were bigger than those of C_3H_8. This was consistent with the single species results discussed in the previous section. Another factor that needs to be taken into consideration is the slope of the calibration line for each species is different. The same amount of change in absorbance represents a bigger variation in concentration for CH_4.

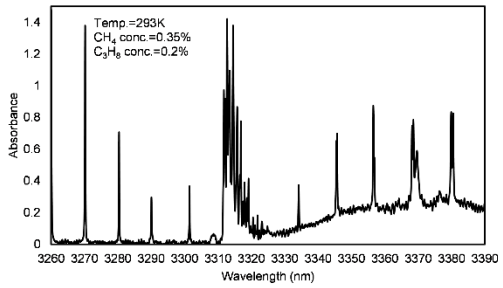

(a) Absorption spectrum of CH_4 and C_3H_8 mixture

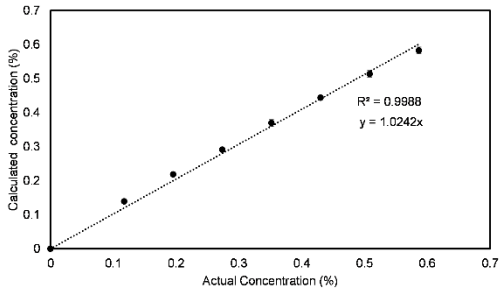

(b) Actual and calculated concentration of CH_4

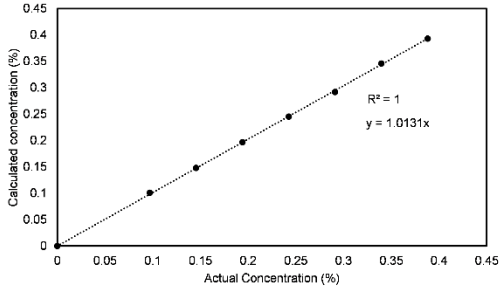

(c) Actual and calculated concentration of C_3H_8

Fig. 4.18 Measurement result of CH_4 and C_3H_8 mixture

The spectra of the C_2H_4 and C_3H_6 mixture was shown in Fig. 4.19(a). Both molecules have absorption peaks in 3346nm and 3384.9nm, respectively. By applying the interferent correction method, the predicted and actual concentrations were depicted in Fig. 4.19(b) and Fig. 4.19(c). The results showed that the influence of overlapping between two molecules was small and the interferent correction method can be applied for quantitative measurement if the components of mixtures are known and pure spectra of single species were measured beforehand.

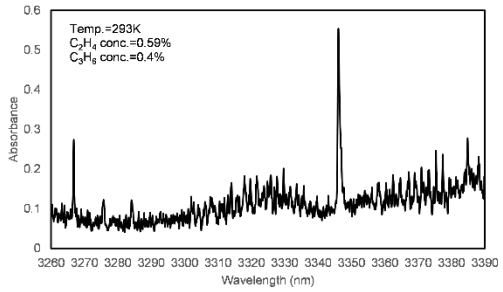

(a) Absorption spectrum of C_2H_4 and C_3H_6 mixture

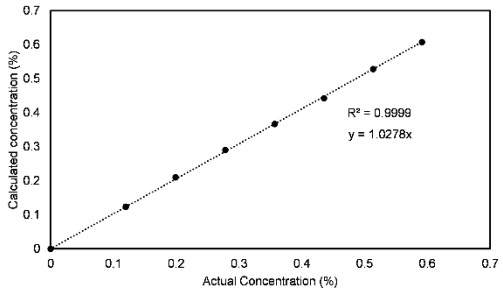

(b) Actual and calculated concentration of C_2H_4

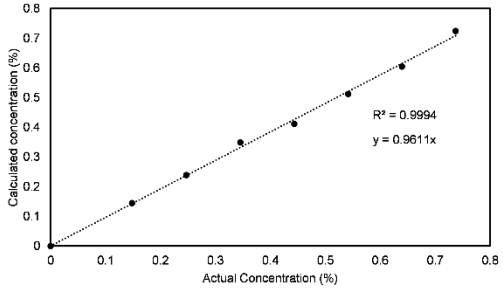

(c) Actual and calculated concentration of C_3H_6

Fig. 4.19 Measurement results of C_2H_4 and C_3H_6

By expanding the experiment to trinary mixtures, we further validated the performance of the system. Fig. 4.20(a) shows the absorption spectrum of CH_4, C_2H_4, and C_3H_8 mixture. The absorption of three species overlaps with each other in the 3310nm-3390nm region while CH_4 has a rather isolated absorption area in 3260-3310nm (with some minor overlapping with C_2H_4). The method applied here was the same as binary mixture measurement. By changing the concentration of one species as the analyte and keep the concentration of the other two the same as the interferent. When CH_4 was the analyte, a peak in 3280.5nm was chosen for analysis. The absorbance in 3280.5nm was used for concentration calculation and the result was compared with the pure CH_4 calibration line. When C_2H_4 and C_3H_8 were the analytes, the interferent correction method was used since the only strong absorption peak of these two species overlap with the interferents. The

absorbance of the mixture at 3336.4nm and 3369.8nm was used to subtract the absorbance of interferents at given concentrations for calculation. The calculated results were illustrated in Fig. 4.20(b), Fig. 4.20(c), and Fig. 4.20(d). The variation in slope and the R^2 values for both C_2H_4 and C_3H_8 measurements were consistent with single species results while a small improvement in CH_4 results was within experimental error.

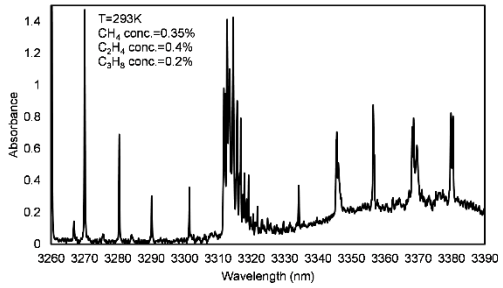

(a) Absorption spectrum of CH_4, C_2H_4 and C_3H_8 mixture

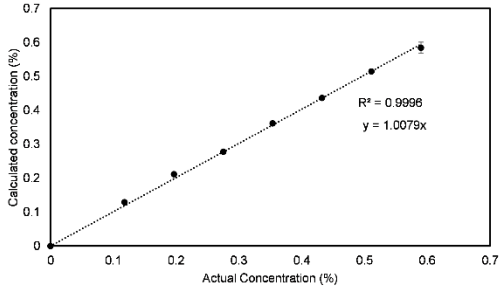

(b) Actual and calculated concentration of CH_4

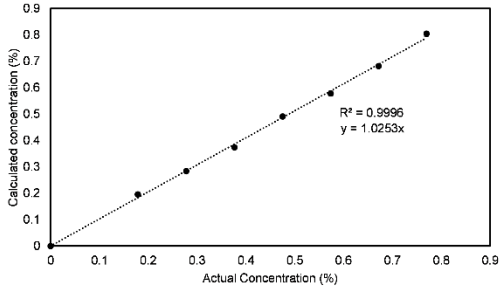

(c) Actual and calculated concentration of C_2H_4

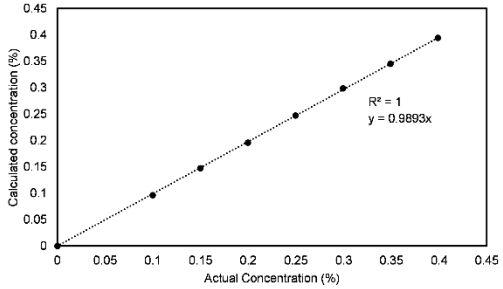

(d) Actual and calculated concentration of C_3H_8

Fig. 4.20 Measurement results of CH_4, C_2H_4 and C_3H_8 mixture

4.2.5 mixture measurement analysis using ICA and CLS methods

The ICA method was applied for the identification of components from the mixture and the CLS method was used for concentration calculations. By using the two methods, it is possible to identify different components within the mixture and determine their concentrations. First the measured mixture spectra were used as input and then the components were separated using the ICA method. Then the spectra of pure species measured at each of their highest concentrations were used together with mixture spectra to calculate the concentrations using the CLS method. The "actual" and "calculated" concentrations were compared and assessed using both the R^2 and the root mean square error of prediction (RMSEP). The term "actual" and "calculated" refer to the known concentration of selected components in the mixture and the value calculated using the CLS method, respectively. The "actual" concentrations were calculated using the readings from the flow meters.

The spectra of several mixtures with certain concentrations were recorded and analyzed. The chosen molecules could cover different absorption shapes. CH_4 and C_2H_4 have narrow sharp peaks, C_3H_6 has absorption in the whole scanning range, C_3H_8 has blunted curve in the longer wavelength region. The chosen mixture sets were divided as partially and fully overlapping with each other.

Two sets of binary mixtures were chosen for validation, one set was CH_4 and C_3H_8 and another was C_2H_4 and C_3H_6. The first set were partially overlapped in the detection wavelength range, and the second set were completely overlapped. Two experiments were carried out for each set. In both experiments, the concentration of one species remains constant while the concentration of the other varies.

The absorption spectra measured in each set were used for ICA decomposition and the components were identified through peak searching and similarity comparison among separated spectra and the spectral database. The separated spectra were displayed in Fig. 4.21(a) and Fig. 4.22(a). All gases were successfully recognized through absorption peaks, and further confirmation was achieved by calculating the correlation coefficient *r* between the pure spectrum and the separated spectrum. The correlation coefficient *r* equation is as follows:

$$r = \frac{\sum[(x_i-\bar{x})*(y_i-\bar{y})]}{\sqrt{\sum[(x_i-\bar{x})^2}*\sqrt{\sum[(y_i-\bar{y})^2}}, i = 1,2,3 \ldots \qquad (4.3)$$

Where x and y represents the datapoints in the two spectra being compared and r>0.9 indicates the two spectra were well matched according to previous study [63]. In the two experiments sets, all values of r were greater than 0.86, showing good separation results using the ICA decomposition method. The separation results for the CH_4 and C_3H_8 set was better than the C_2H_4 and C_3H_6 set, which can be explained by the complex absorption structure and overlapped absorption bands. The identification results were summarized in Table 6.

Table 6 Species identification results for mixtures

Mixture Set	Species	Absorption Peak (nm)	Correlation coefficients
CH_4 and C_3H_8	CH_4	3313.7	0.9502
	C_3H_8	3369.7	0.9653
C_2H_4 and C_3H_6	C_2H_4	3346.2	0.9106
	C_3H_6	3384.7	0.8689
CH_4, C_2H_4, and C_3H_8	CH_4	3313.7	0.9881
	C_2H_4	3346.2	0.8967
	C_3H_8	3369.7	0.9885

After species identification, quantitative analysis was performed using the CLS method to determine the variation in concentration. The calculation results using the CLS method were displayed in Fig. 4.21(b) and Fig. 4.21(c). The R^2 values obtained for CH_4 and C_3H_8 respectively were 0.9992 and 0.9999, RMSEP values were 0.012% and 0.008%. Both values indicate good linearity and a small variance between actual and calculated concentrations.

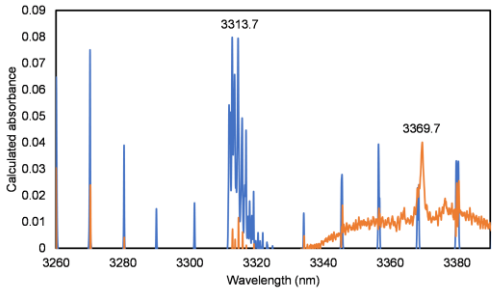

(a) Separated results of CH_4 and C_3H_8 mixture

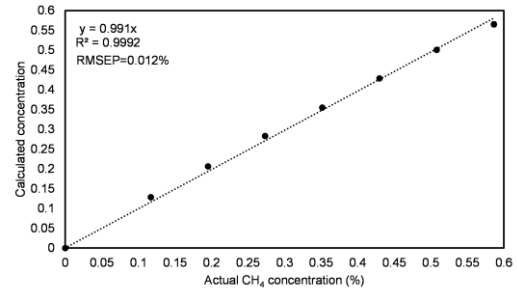

(b) Actual and calculated concentration of CH_4

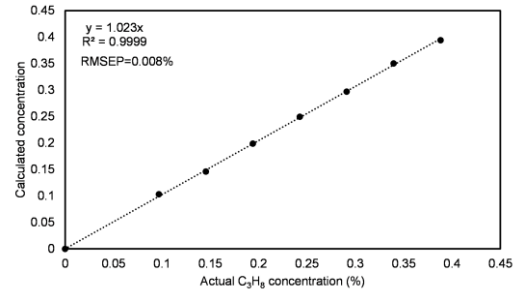

(c) Actual and calculated concentration of C_3H_8

Fig. 4.21 Measurement result of CH_4 and C_3H_8 mixture

The spectra and results for C_2H_4 and C_3H_6 were shown in Fig. 4.22. The R^2 values for C_2H_4 and C_3H_6 were 0.9981 and 0.9985, RMSEP values were 0.033% and 0.029%. Both values also indicate good fitting results although the results for CH_4 and C_3H_8 were better. The overlapping between these two molecules might influence the mixture spectra that worsen the fitting result. The concentration dependence results for C_3H_6 showed more uncertainty since the calculation used the pure spectra of single species, this could also affect the mixture detection results.

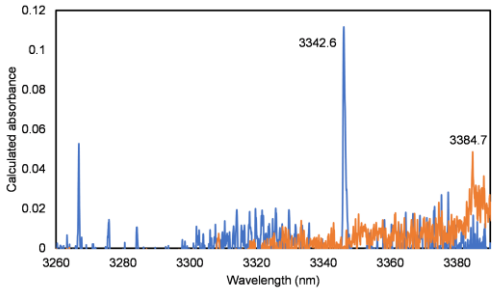

(a) Separated results of C_2H_4 and C_3H_6 mixture

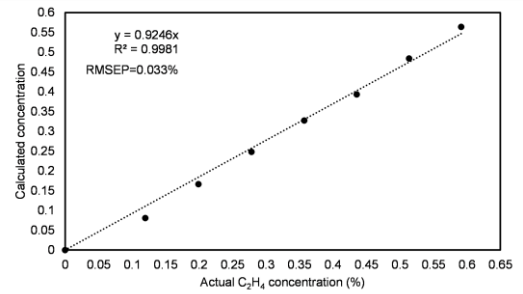

(b) Actual and calculated concentration of C_2H_4

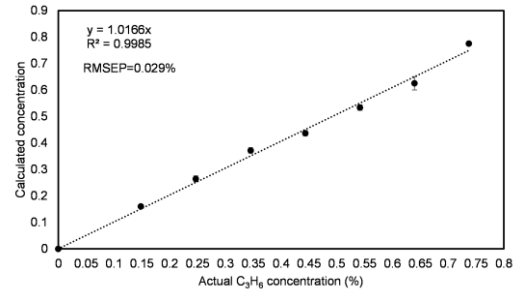

(c) Actual and calculated concentration of C_3H_6

Fig. 4.22 Measurement results of C_2H_4 and C_3H_6

By expanding the experiment to trinary mixtures, the performance of the system was further validated. Peak searching was first performed for the separated spectra and all three species were identified. The *r* values for CH_4, C_2H_4, and C_3H_8 were 0.988, 0.896, and 0.989, respectively as shown in Fig. 4.23. The C_2H_4 correlation was the lowest, which was consistent with the binary measurement results.

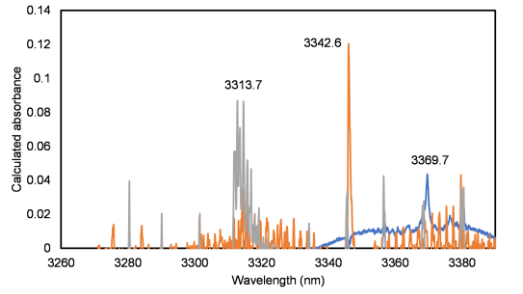

(a) Separated results of CH_4, C_2H_4 and C_3H_8 mixture

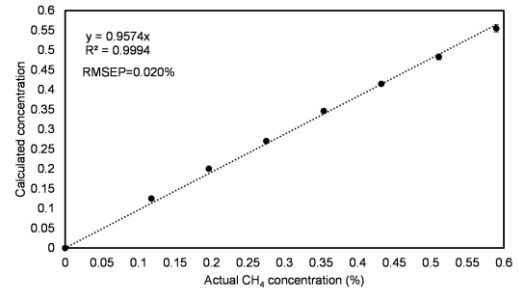

(b) Actual and calculated concentration of CH_4

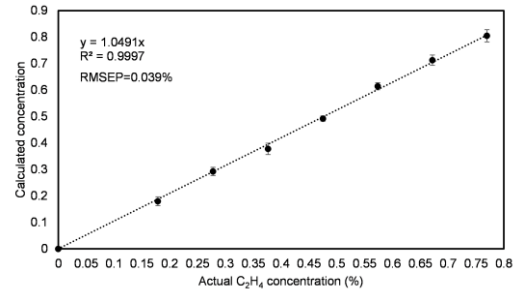

(c) Actual and calculated concentration of C_2H_4

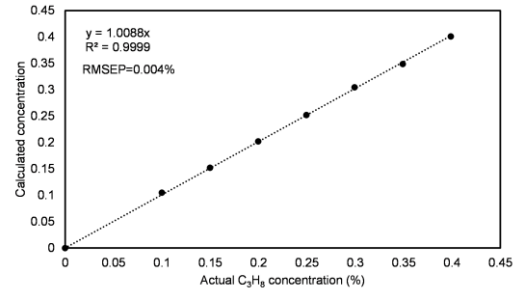

(d) Actual and calculated concentration of C_3H_8

Fig. 4.23 Measurement results of CH_4, C_2H_4 and C_3H_8 mixture

The calculated concentration results were illustrated in Fig. 4.23(b), Fig. 4.23(c), and Fig. 4.23(d). For CH_4, the R^2 and RMSEP values were 0.9994 and 0.020%, which was a little worse than the CH_4 and C_3H_8 mixture measurement result. For C_2H_4 and C_3H_8, the results were almost identical to binary mixture detection, with the R^2 values 0.9997 and 0.9999, the RMSEP values 0.039% and 0.004% for each species. With the presence of another interferent in mixtures, only small changes were observed compared to binary mixture measurements. Overall, the high R^2 and low RMSEP values proved the CLS method is reliable in predicting the concentration of mixture components.

The experiments being carried out were able to prove the proposed system is capable of mixture hydrocarbon measurements. The results suggest the ICA and the CLS method can be used to

identify species in the mixture and quantitatively determine the concentration of different components without the need to find isolated absorption peaks.

4.3 Engine exhaust measurement result

Engine's rotation speed and temperature results measured by a tachometer and a thermocouple were displayed in Fig. 4.24.

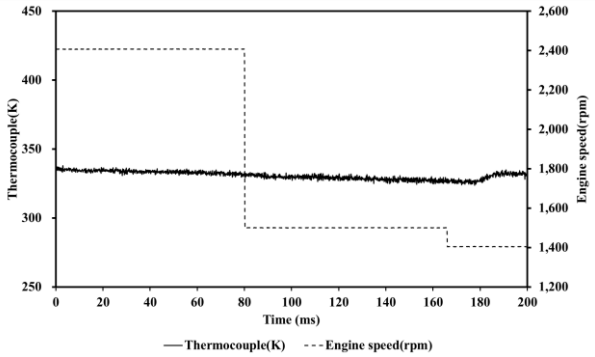

Fig. 4.24 Results of thermocouple temperature and engine speed

Engine was started in idle status and measurement lasts 200ms after engine started. The start threshold of measurement was set according to rotation speed (1800rpm).

Absorption spectra at different time was illustrated in Fig. 4.25.

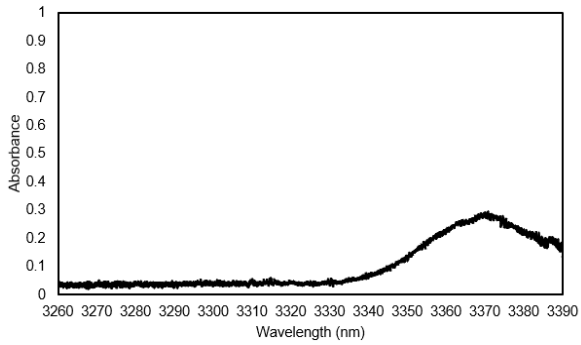

(a) 0-20ms

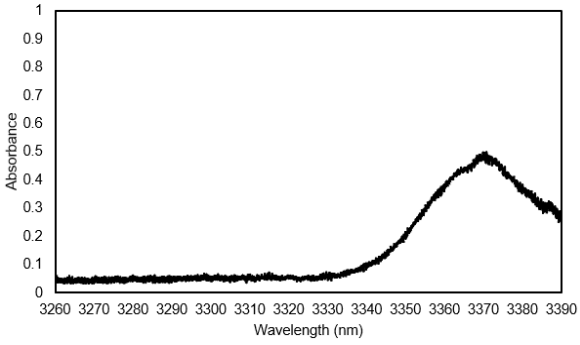

(b) 20-40ms

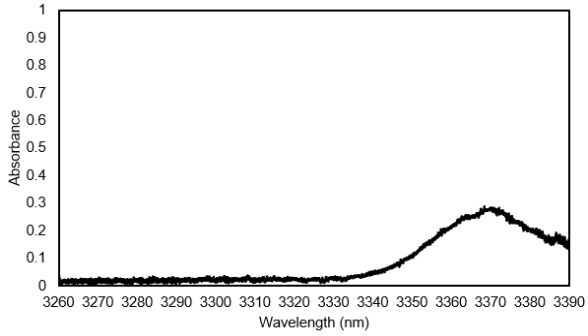

(c) 40-60ms

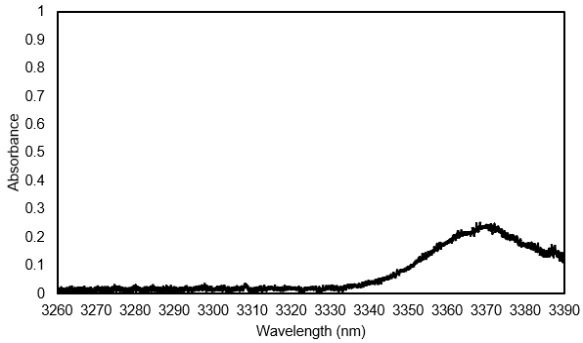

(d) 60-80msms

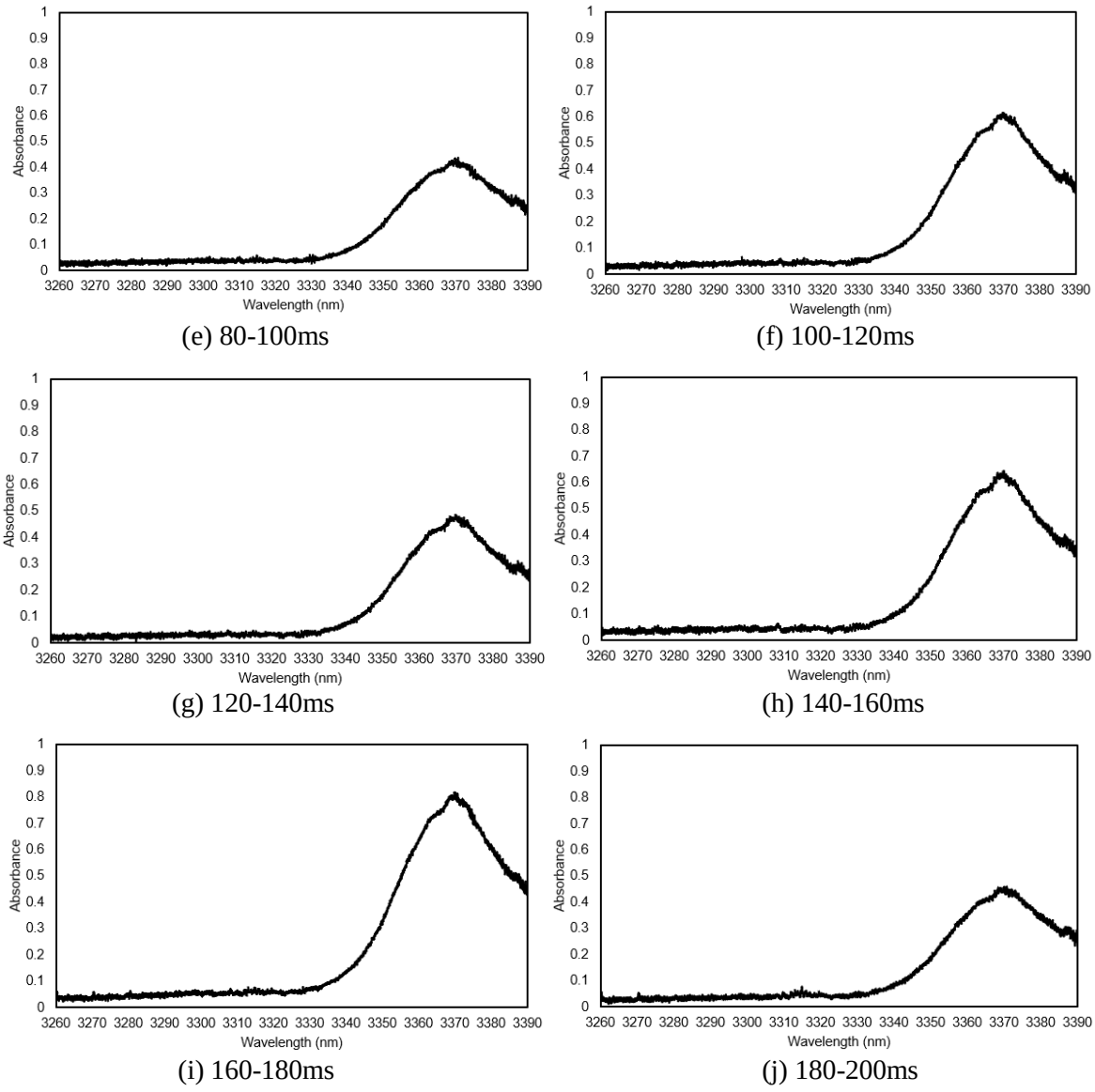

(e) 80-100ms (f) 100-120ms

(g) 120-140ms (h) 140-160ms

(i) 160-180ms (j) 180-200ms

Fig.4.25 Absorption spectra in engine exhausts at different time

First, a visual check was performed to analyze the potential hydrocarbons. As can be seen from the spectra, during the whole 200ms time period, clear absorption in the wavelength range bigger than 3330nm can be observed. This indicates the existence of relatively large amount of aliphatic hydrocarbon. While the absorption in the wavelength smaller than 3330nm was trivial, which means the amount of aromatic hydrocarbon was small. The spectra also lack clear isolated sharp absorption peaks, this means that the number of light molecules like CH_4, C_2H_4 and C_2H_6 were also small and need further analysis to confirm their existence.

The peak absorbance height change in the wavelength around 3370nm can also be seen clearly, showing the change in hydrocarbon concentrations according to time. This indicates the laser system can monitor the real-time processes in short time intervals due to its high frequency.

For quantitative analysis, the least squares regression was performed. The method has been discussed in the previous chapter. The ICA approach was not used to separate the signals as the method requires the components of the source signal to be statistically independent. But in this situation, this prerequisite was not met (the concentrations of hydrocarbons tend to change together) and the decomposition results was not ideal.

To perform the least squares regression, the pure hydrocarbons spectra measured beforehand were used as a database and was fitted to the measured spectra. An example of the results was shown in Fig. 4.26.

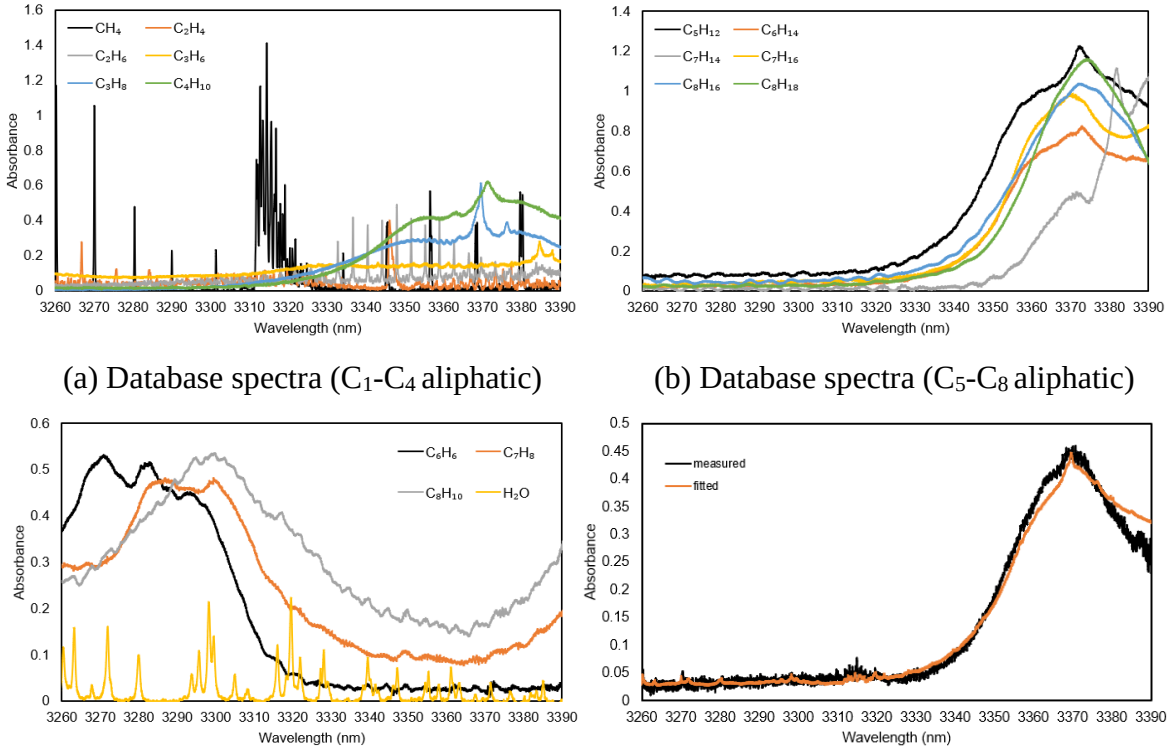

(a) Database spectra (C_1-C_4 aliphatic) (b) Database spectra (C_5-C_8 aliphatic)

(c) Database spectra (aromatic and H_2O) (d) Measured and fitted spectra (180-200ms)

Fig. 4.26 Fitting spectra using the spectra database

Ten spectra were fitted using the same method. To evaluate the performance, the values of R^2 were also used. A minimum of 0.976 and maximum of 0.984 was achieved, indicating good fitting performance. The calculated concentration results for each time period were shown in Fig. 4.27.

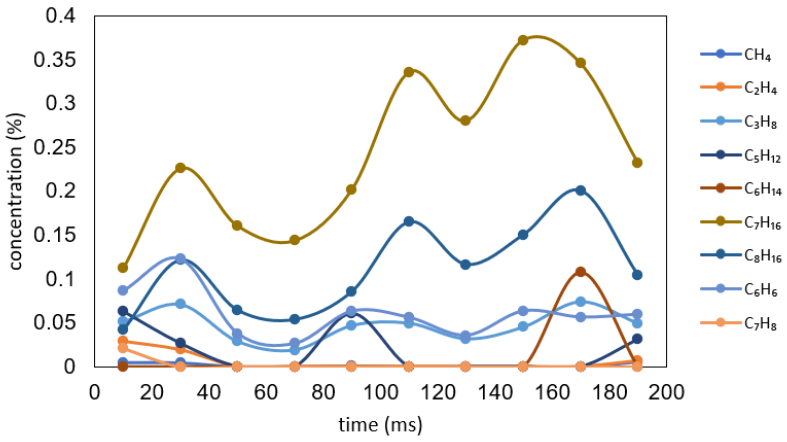

Fig. 4.27 Calculated concentrations at different time

By comparing the calculated concentration to the detection of limit, numbers that were too small were discarded or treat as zero. Totally nine out of fifteen species were recognized. The most abundant species were C_7H_{16} and C_8H_{16}, which consist of the big absorption peaks in the wavelength region larger than 3300nm. C_3H_8 and C_6H_6 also appeared in the whole measurement period. Only Small amount of CH_4, C_2H_4 and C_7H_8 appeared in the beginning and C_5H_{12} appeared during the intervals.

Despite the good fitting results, the temperature conditions were different between the database and the actual condition, and in actual conditions, the number of hydrocarbons tend to be bigger than our database, so the fitting result was an approximation and can be improved by further expanding our database in the aspect of the number of hydrocarbons and the number of different temperature conditions.

4.4 Low-temperature coal pyrolysis process measurement result

In most coal conversion processes like combustion, gasification, and liquefaction, pyrolysis is an important step [64]. Pyrolysis occurs at temperature up to about 700℃ where light gases (such as H_2O, CH_4, CO), tar and char are released. When temperature is under 400℃, the volatiles mainly come from evaporation rather than degradation [65].

The spectra of multiple pure hydrocarbon molecules belonging to different classes have already been recorded beforehand. Light hydrocarbons (smaller than C_3) and water vapor have sharp distinguishable absorption peaks, while heavier molecules have more blunted spectra patterns. A general identification of the measurement results was made by comparing the measured results with current pure hydrocarbon spectroscopic database. Fig. 4.28 showed the spectra of the pure hydrocarbons identified in the measurement. The spectra were recorded after the valves of the

absorbing cell were opened and gas flowed through the cell for one minute. When coal samples were heated to 100℃ and 150℃, only water vapor was observed from the spectra. When temperature was raised to 200℃, more absorption occurred in the 3360-3390nm region, indicating the release of heavier aliphatic hydrocarbons. When the temperature was up to 250℃, more heavy hydrocarbons were released as the absorption in the longer wavelength continues to become bigger. After the temperature was above 300℃, clear absorption peaks of CH_4 and C_2H_6 were found, as shown in Fig. 4.28(e) and Fig. 4.28(f). The aromatic hydrocarbons usually have absorption in the wavelength region smaller than 3320nm, and this was also observed when the coal sample was heated over 300℃.

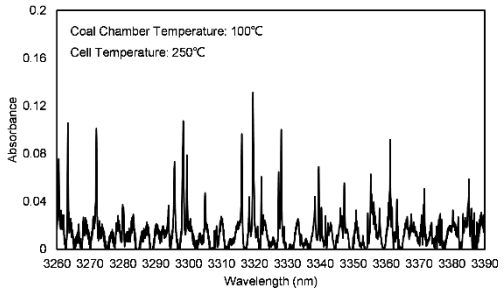

(a) Absorption spectra at 100℃

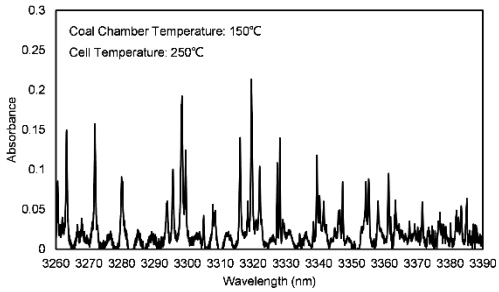

(b) Absorption spectra at 150℃

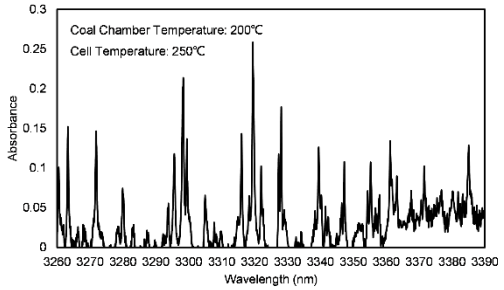

(c) Absorption spectra at 200℃

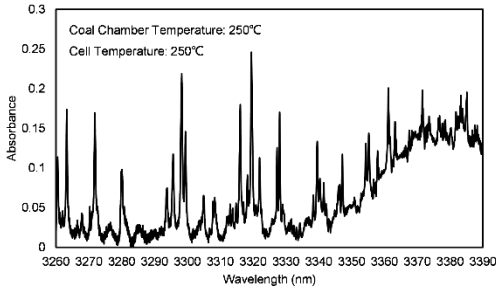

(d) Absorption spectra at 250℃

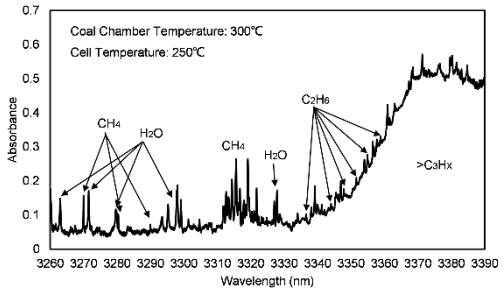

(e) Absorption spectra at 300℃

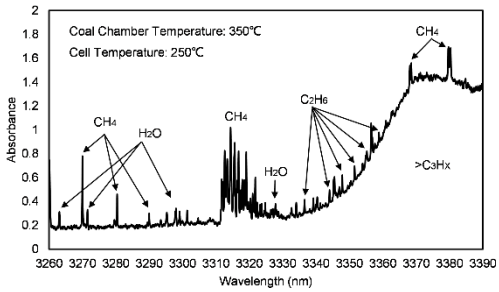

(f) Absorption spectra at 350℃

Fig. 4.28 Absorption spectra of coal pyrolysis at different temperature ℃

For quantitative analysis of the results, the least-squares fitting of the spectra was performed. The method has already been used by our group for separating hydrocarbon mixture at given conditions and proved its reliability. By using the measured pure hydrocarbon spectra at given concentration and temperature, the concentration of each potential component within the mixture was calculated. Least-squares fittings were performed for heated temperature higher than 200℃. The measured and fitted spectra at heated temperature of 350℃ were both shown in Fig. 4.29.

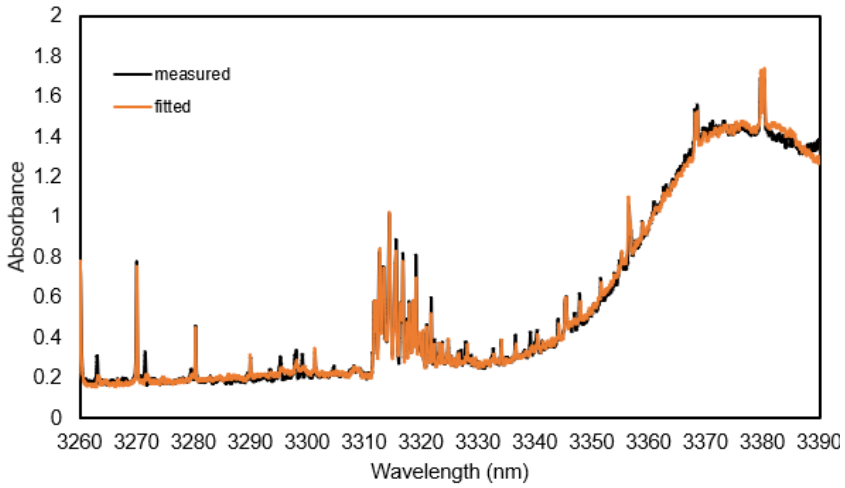

Fig. 4.29 Measured and fitted spectra at

The R^2 value was used to assess the quality between the measured data and the model. The R^2 value close to 1 indicates the linear regression of the data is good with small variance. The experiments were performed three times and the R^2 values for the other two times at 350℃ were 0.996 and 0.995, showing good fitting performance. The minimum R^2 value of 0.889 appeared at 250℃. The bigger absorbance will lead to better fitting result since the influence of noise was smaller.

By using the least-squares fitting method, the concentration for each component in the mixture was calculated and the result was shown in Fig. 4.30. The water vapor was considered as an interference species and the concentration was not included in the figure.

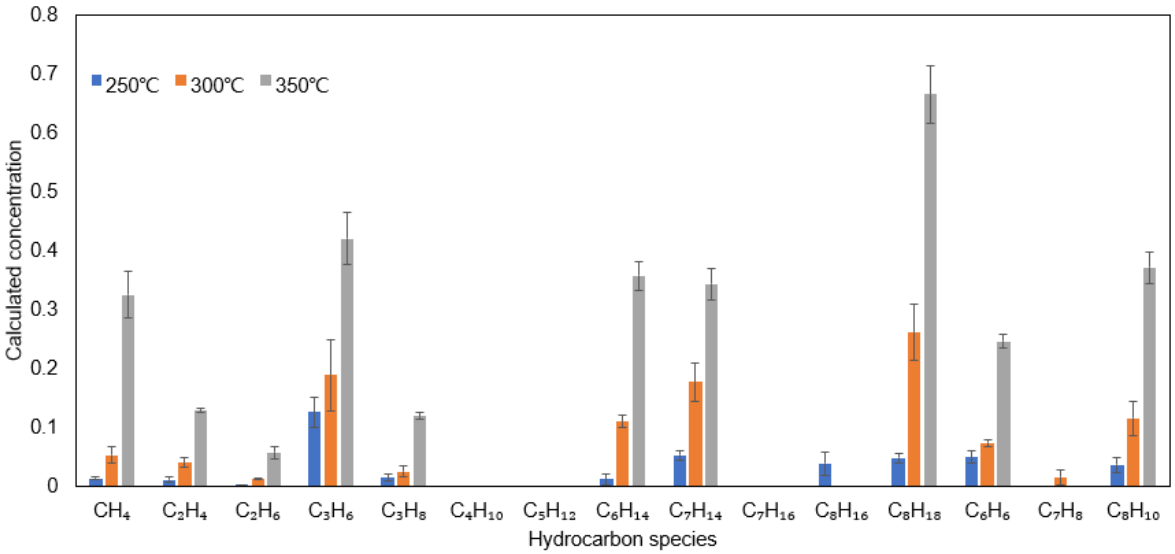

Fig. 4.30 Calculated concentration of each species using the fitted data

According to the calculation results, twelve hydrocarbon species out of the total fifteen species database were detected. Despite of C_8H_{16} and C_7H_8, all the molecules being detected appear at all three temperature and the concentration increases as the temperature goes up. C_8H_{16} was only calculated in 250℃ while C_7H_8 only in 300℃ and both only appeared in one measurement. We could infer that these species could be ruled out in the calculation.

The coal pyrolysis is a complicate process with many gaseous and oil products [4], [66], [67]. The current fitting result was a demonstration of the approach and better results could be achieved if the database were enlarged by more hydrocarbon spectra.

5 Conclusions

In this work, a DFG laser was used for hydrocarbon detection and laser system was applied to engine exhaust measurement and coal powder measurement.

According to experiment results, conclusions are drawn as follows.

1) Hydrocarbon measurement using a DFG laser

The absorption spectra of fifteen different hydrocarbon molecules ranging from C1 to C8 were probed. Results of the concentration dependence of absorbance were obtained for each molecule. Linear dependence results with the R2 values larger than 0.997 demonstrated the system was able to measure hydrocarbons covering different molecular classes accurately. The measurement of methane at different temperatures confirmed the nonlinear relationship between temperature and absorbance.

Mixtures of hydrocarbon gases measurements from binary to trinary mixtures were performed to validate the performance of the system on mixture detection, which is important in actual applications. The values of r larger than 0.86 showed that the ICA algorithm can effectively achieve mixture separation. The R2 values higher than 0.998 and RMSEP values smaller than 0.04% proved that the CLS method can be applied to predict the concentrations of target species in the mixture by using the spectra of pure species.

2) Engine exhaust measurement

Engine exhaust was detected, and the spectra were recorded. The recorded spectra were analyzed at a 20ms gap based on the rotation speed of the engine. The change in absorbance was clearly observed at different time gap, which proved the capability of the laser system on real-time measurement. The spectra were also analyzed using the fitting method and ten hydrocarbon molecules were recognized. It was shown that both light hydrocarbon molecules like CH_4 and heavier hydrocarbon molecules exist in exhaust gas, which showed the possibility of this laser system in analyzing the combustion process from exhaust gas in short time interval (millisecond level).

3) Coal powder measurement

Coal powder samples were heated from 100℃ to 350℃ at a constant 50℃ interval. The release of aliphatic hydrocarbon gases started above 200℃, small hydrocarbon molecules like CH_4 and C_2H_6 was detected above 250℃ and aromatic hydrocarbons appeared when temperature was over 300℃. The spectra fourteen pure hydrocarbon was heated to four discrete temperatures between 150℃ and 450℃ and the spectra were recorded as database. Based on the database, least-squares fitting was performed, with a minimum R^2 value of 0.953 which shows small variance between fitted and measured spectra. Eleven different hydrocarbon molecules were identified quantitatively. By examining different temperature stages, the laser system can help clarifying the chemical

process during coal's pyrolysis and the volatilization and formation of different hydrocarbon components.

Overall, the proposed system is a good candidate for industrial hydrocarbon detection by overcoming the limitation of other tunable diode lasers designed for hydrocarbon measurement while maintaining its advantages. The two actual experiments proved the proposed laser system can detect multiple hydrocarbons simultaneously in actual situations. Further study is needed on acquiring the spectra of more hydrocarbons which could exist from the processes being measured and other analysis methods could be applied for better fitting results.

References

[1] J. Liu, X. Jiang, J. Shen, and H. Zhang, "Pyrolysis of superfine pulverized coal. Part 1. Mechanisms of methane formation," *Energy Convers. Manag.*, vol. 87, pp. 1027–1038, 2014, doi: 10.1016/j.enconman.2014.07.053.

[2] M. A. Serio, D. G. Hamblen, J. R. Markham, and P. R. Solomon, "Kinetics of Volatile Product Evolution in Coal Pyrolysis: Experiment and Theory," *Energy and Fuels*, vol. 1, no. 2, pp. 138–152, 1987, doi: 10.1021/ef00002a002.

[3] Z. Niu, G. Liu, H. Yin, D. Wu, and C. Zhou, "Investigation of mechanism and kinetics of non-isothermal low temperature pyrolysis of perhydrous bituminous coal by in-situ FTIR," *Fuel*, vol. 172, pp. 1–10, 2016, doi: 10.1016/j.fuel.2016.01.007.

[4] M. Wang, Z. Li, W. Huang, J. Yang, and H. Xue, "Coal pyrolysis characteristics by TG-MS and its late gas generation potential," *Fuel*, vol. 156, pp. 243–253, 2015, doi: 10.1016/j.fuel.2015.04.055.

[5] Q. He, K. Wan, A. Hoadley, H. Yeasmin, and Z. Miao, "TG-GC-MS study of volatile products from Shengli lignite pyrolysis," *Fuel*, vol. 156, no. April, pp. 121–128, 2015, doi: 10.1016/j.fuel.2015.04.043.

[6] A. Arenillas, C. Pevida, F. Rubiera, R. García, and J. J. Pis, "Characterisation of model compounds and a synthetic coal by TG/MS/FTIR to represent the pyrolysis behaviour of coal," *J. Anal. Appl. Pyrolysis*, vol. 71, no. 2, pp. 747–763, 2004, doi: 10.1016/j.jaap.2003.10.005.

[7] L. Jia, J. Weng, Y. Wang, S. Sun, Z. Zhou, and F. Qi, "Online Analysis of Volatile Products from Bituminous Coal Pyrolysis with Synchrotron Vacuum Ultraviolet Photoionization Mass Spectrometry," *Energy & Fuels*, vol. 27, no. 2, pp. 694–701, Feb. 2013, doi: 10.1021/ef301670y.

[8] R. Sur, S. Wang, K. Sun, D. F. Davidson, J. B. Jeffries, and R. K. Hanson, "High-sensitivity interference-free diagnostic for measurement of methane in shock tubes," *J. Quant. Spectrosc. Radiat. Transf.*, vol. 156, pp. 80–87, 2015, doi: 10.1016/j.jqsrt.2015.01.023.

[9] K. Krzempek *et al.*, "Continuous wave, distributed feedback diode laser based sensor for trace-gas detection of ethane," *Appl. Phys. B Lasers Opt.*, vol. 106, no. 2, pp. 251–255, 2012, doi: 10.1007/s00340-011-4857-9.

[10] P. Kluczynski *et al.*, “Detection of propane using tunable diode laser spectroscopy at 3.37 μm,” *Appl. Phys. B Lasers Opt.*, vol. 108, no. 1, pp. 183–188, 2012, doi: 10.1007/s00340-012-5054-1.

[11] N. Lang, U. Macherius, M. Wiese, H. Zimmermann, J. Röpcke, and J. H. van Helden, “Sensitive CH_4 detection applying quantum cascade laser based optical feedback cavity-enhanced absorption spectroscopy,” *Opt. Express*, vol. 24, no. 6, p. A536, 2016, doi: 10.1364/oe.24.00a536.

[12] Y. Cao *et al.*, “Simultaneous atmospheric nitrous oxide, methane and water vapor detection with a single continuous wave quantum cascade laser,” *Opt. Express*, vol. 23, no. 3, p. 2121, 2015, doi: 10.1364/oe.23.002121.

[13] L. Dong *et al.*, “Compact TDLAS based sensor design using interband cascade lasers for mid-IR trace gas sensing,” *Opt. Express*, vol. 24, no. 6, p. A528, 2016, doi: 10.1364/oe.24.00a528.

[14] S. Wang, T. Parise, S. E. Johnson, D. F. Davidson, and R. K. Hanson, “A new diagnostic for hydrocarbon fuels using 3.41-μm diode laser absorption,” *Combust. Flame*, vol. 186, pp. 129–139, 2017, doi: 10.1016/j.combustflame.2017.07.026.

[15] A. Sampaolo *et al.*, “Methane, ethane and propane detection using a compact quartz enhanced photoacoustic sensor and a single interband cascade laser,” *Sensors Actuators, B Chem.*, vol. 282, no. November 2018, pp. 952–960, 2019, doi: 10.1016/j.snb.2018.11.132.

[16] K. P. Petrov *et al.*, “Precise measurement of methane in air using diode-pumped 3.4-μm difference-frequency generation in PPLN,” *Appl. Phys. B Lasers Opt.*, vol. 64, no. 5, pp. 567–572, 1997, doi: 10.1007/s003400050216.

[17] D. Richter, D. G. Lancaster, R. F. Curl, W. Neu, and F. K. Tittel, “Compact mid-infrared trace gas sensor based on difference-frequency generation of two diode lasers in periodically poled LiNbO3,” *Appl. Phys. B Lasers Opt.*, vol. 67, no. 3, pp. 347–350, 1998, doi: 10.1007/s003400050514.

[18] U. Gustafsson, J. Sandsten, and S. Svanberg, “Simultaneous detection of methane, oxygen and water vapour utilising near-infrared diode lasers in conjunction with difference-frequency generation,” *Appl. Phys. B Lasers Opt.*, vol. 71, no. 6, pp. 853–857, 2000, doi: 10.1007/s003400000431.

[19] K. Liu *et al.*, “Highly sensitive detection of methane by near-infrared laser absorption spectroscopy using a compact dense-pattern multipass cell,” *Sensors Actuators, B Chem.*, vol. 220, pp. 1000–1005, 2015, doi: 10.1016/j.snb.2015.05.136.

[20] M. E. Trudeau, P. Chen, G. A. De Garcia, L. W. Hollberg, and P. P. Tans, “Stable isotopic analysis of atmospheric methane by infrared spectroscopy by use of diode laser difference-frequency generation,” *Appl. Opt.*, vol. 45, no. 17, pp. 4136–4141, 2006, doi: 10.1364/AO.45.004136.

[21] A. E. Klingbeil, J. B. Jeffries, and R. K. Hanson, “Tunable mid-IR laser absorption sensor for time-resolved hydrocarbon fuel measurements,” *Proc. Combust. Inst.*, vol. 31 I, no. 1, pp. 807–815, 2007, doi: 10.1016/j.proci.2006.07.228.

[22] J. Hodgkinson and R. P. Tatam, “Optical gas sensing: a review,” *Meas. Sci. Technol.*, vol. 24, no. 1, p. 12004, 2012, doi: 10.1088/0957-0233/24/1/012004.

[23] D. Richter, A. Fried, and P. Weibring, “Difference frequency generation laser based spectrometers,” *Laser Photonics Rev.*, vol. 3, no. 4, pp. 343–354, 2009, doi: 10.1002/lpor.200810048.

[24] N. P. Barnes, “Optical parametric oscillators,” *Tunable lasers Handb.*, pp. 293–348, 1995.

[25] J. Faist, F. Capasso, D. L. Sivco, C. Sirtori, A. L. Hutchinson, and A. Y. Cho, “Quantum cascade laser,” *Science (80-.).*, vol. 264, no. 5158, pp. 553–556, 1994.

[26] E. D. Hinkley, K. W. Nill, and F. A. Blum, “Infrared spectroscopy with tunable lasers,” in *Laser spectroscopy of atoms and molecules*, Springer, 1976, pp. 125–196.

[27] E. Hirota, *High-resolution spectroscopy of transient molecules*, vol. 40. Springer Science \& Business Media, 2012.

[28] L. Hollberg, “Diode Lasers and their Application to Spectroscopy,” in *Applied Laser Spectroscopy*, Springer, 1990, pp. 117–125.

[29] S. Civiš, J. Cihelka, and I. Matulková, “Infrared diode laser spectroscopy,” *Opto-Electronics Rev.*, vol. 18, no. 4, pp. 408–420, 2010.

[30] F. K. Tittel, D. Richter, and A. Fried, “Mid-infrared laser applications in spectroscopy,” *Solid-state mid-infrared laser sources*, pp. 458–529, 2003.

[31] T. Schilling, F.-J. Lübken, F. G. Wienhold, P. Hoor, and H. Fischer, “TDLAS trace gas measurements within mountain waves over northern Scandinavia during the POLSTAR campaign in early 1997,” *Geophys. Res. Lett.*, vol. 26, no. 3, pp. 303–306, 1999.

[32] L. Dong *et al.*, “Compact TDLAS based sensor design using interband cascade lasers for mid-IR trace gas sensing,” *Opt. Express*, vol. 24, no. 6, pp. A528--A535, 2016, doi: 10.1364/OE.24.00A528.

[33] J. Röpcke, G. Lombardi, A. Rousseau, and P. B. Davies, “Application of mid-infrared tuneable diode laser absorption spectroscopy to plasma diagnostics: a review,” *Plasma Sources Sci. Technol.*, vol. 15, no. 4, p. S148, 2006.

[34] J. Röpcke, P. B. Davies, N. Lang, A. Rousseau, and S. Welzel, “Applications of quantum cascade lasers in plasma diagnostics: a review,” *J. Phys. D. Appl. Phys.*, vol. 45, no. 42, p. 423001, 2012.

[35] M. G. Allen, “Diode laser absorption sensors for gas-dynamic and combustion flows,” *Meas. Sci. Technol.*, vol. 9, no. 4, p. 545, 1998.

[36] M. A. Bolshov, Y. A. Kuritsyn, and Y. V Romanovskii, “Tunable diode laser spectroscopy as a technique for combustion diagnostics,” *Spectrochim. Acta Part B At. Spectrosc.*, vol. 106, pp. 45–66, 2015.

[37] R. K. Hanson, “Applications of quantitative laser sensors to kinetics, propulsion and practical energy systems,” *Proc. Combust. Inst.*, vol. 33, no. 1, pp. 1–40, 2011.

[38] Y. Deguchi, *Industrial applications of laser diagnostics*. CRC Press, 2011.

[39] I. E. Gordon *et al.*, “The HITRAN2016 molecular spectroscopic database,” *J. Quant. Spectrosc. Radiat. Transf.*, vol. 203, pp. 3–69, 2017, doi: 10.1016/j.jqsrt.2017.06.038.

[40] A. M. Kelley, *Condensed-phase molecular spectroscopy and photophysics*. Wiley Online Library, 2013.

[41] S. R. Drayson, “Rapid computation of the Voigt profile,” *J. Quant. Spectrosc. Radiat. Transf.*, vol. 16, no. 7, pp. 611–614, 1976.

[42] R. J. Wells, “Rapid approximation to the Voigt/Faddeeva function and its derivatives,” *J. Quant. Spectrosc. Radiat. Transf.*, vol. 62, no. 1, pp. 29–48, 1999.

[43] E. E. Whiting, “An empirical approximation to the Voigt profile,” *J. Quant. Spectrosc. Radiat. Transf.*, vol. 8, no. 6, pp. 1379–1384, 1968.

[44] Y. B. Monakhova, S. A. Astakhov, A. Kraskov, and S. P. Mushtakova, “Independent components in spectroscopic analysis of complex mixtures,” *Chemom. Intell. Lab. Syst.*, vol. 103, no. 2, pp. 108–115, 2010, doi: 10.1016/j.chemolab.2010.05.023.

[45] G. Wang, Q. Ding, and Z. Hou, “Independent component analysis and its applications in signal processing for analytical chemistry,” *TrAC - Trends Anal. Chem.*, vol. 27, no. 4, pp. 368–376, 2008, doi: 10.1016/j.trac.2008.01.009.

[46] X. Yu *et al.*, “Discrimination of three dimensional fluorescence spectra based on wavelet analysis and independent component analysis,” *Spectrochim. Acta - Part A Mol. Biomol. Spectrosc.*, vol. 124, pp. 52–58, 2014, doi: 10.1016/j.saa.2013.12.033.

[47] L. De Lathauwer, B. De Moor, and J. Vandewalle, “An introduction to independent component analysis,” *J. Chemom. A J. Chemom. Soc.*, vol. 14, no. 3, pp. 123–149, 2000.

[48] P. Comon, C. Jutten, and J. Herault, “Blind separation of sources, Part II: Problems statement,” *Signal Processing*, vol. 24, no. 1, pp. 11–20, 1991.

[49] A. Hyvärinen and E. Oja, “A fast fixed-point algorithm for independent component analysis,” *Neural Comput.*, vol. 9, no. 7, pp. 1483–1492, 1997.

[50] R. Kramer, *Chemometric Techniques for Quantitative Analysis*. CRC Press, 1998.

[51] S. M. Sarathy, A. Farooq, and G. T. Kalghatgi, “Recent progress in gasoline surrogate fuels,” *Prog. Energy Combust. Sci.*, vol. 65, pp. 67–108, 2018, doi: 10.1016/j.pecs.2017.09.004.

[52] L. S. Rothman *et al.*, “HITEMP, the high-temperature molecular spectroscopic database,” *J. Quant. Spectrosc. Radiat. Transf.*, vol. 111, no. 15, pp. 2139–2150, 2010, doi: 10.1016/j.jqsrt.2010.05.001.

[53] T. J. Johnson, R. L. Sams, and S. W. Sharpe, “The PNNL quantitative infrared database for gas-phase sensing: a spectral library for environmental, hazmat, and public safety standoff detection,” in *Chemical and Biological Point Sensors for Homeland Defense*, 2004, vol. 5269, pp. 159–167.

[54] K. C. Cossel, E. M. Waxman, I. A. Finneran, G. A. Blake, J. Ye, and N. R. Newbury, “Gas-phase broadband spectroscopy using active sources: progress, status, and applications [Invited],” *J. Opt. Soc. Am. B*, vol. 34, no. 1, p. 104, 2017, doi: 10.1364/josab.34.000104.

[55] M. Abe, K. Iwakuni, S. Okubo, and H. Sasada, “Accurate transition frequency list of the v3 band of methane from sub-Doppler resolution comb-referenced spectroscopy,” *J. Opt. Soc. Am. B*, vol. 30, no. 4, pp. 1027–1035, 2013, doi: 10.1364/JOSAB.30.001027.

[56] M. Bach, R. Georges, M. Hepp, and M. Herman, “Slit-jet Fourier transform infrared spectroscopy in 12C2H4 : Cold and hot bands near 3000 cm-1,” *Chem. Phys. Lett.*, vol. 294, no. 6, pp. 533–537, 1998, doi: 10.1016/S0009-2614(98)00889-6.

[57] J. J. Harrison, N. D. C. Allen, and P. F. Bernath, “Infrared absorption cross sections for ethane (C2H6) in the 3 μm region,” *J. Quant. Spectrosc. Radiat. Transf.*, vol. 111, no. 3, pp. 357–363, 2010, doi: 10.1016/j.jqsrt.2009.09.010.

[58] J. J. Harrison and P. F. Bernath, “Infrared absorption cross sections for propane (C3H8) in the 3μm region,” *J. Quant. Spectrosc. Radiat. Transf.*, vol. 111, no. 9, pp. 1282–1288, 2010, doi: 10.1016/j.jqsrt.2009.11.027.

[59] A. E. Klingbeil, J. B. Jeffries, and R. K. Hanson, “Temperature-dependent mid-IR absorption spectra of gaseous hydrocarbons,” *J. Quant. Spectrosc. Radiat. Transf.*, vol. 107, no. 3, pp. 407–420, 2007, doi: 10.1016/j.jqsrt.2007.03.004.

[60] C. P. Rinsland, V. M. Devi, T. A. Blake, R. L. Sams, S. Sharpe, and L. Chiou, “Quantitative measurement of integrated band intensities of benzene vapor in the mid-infrared at 278, 298, and 323 K,” *J. Quant. Spectrosc. Radiat. Transf.*, vol. 109, no. 15, pp. 2511–2522, 2008, doi: 10.1016/j.jqsrt.2008.04.007.

[61] L. Pele, J. Šebek, E. O. Potma, and R. Benny Gerber, “Raman and IR spectra of butane: Anharmonic calculations and interpretation of room temperature spectra,” *Chem. Phys. Lett.*, vol. 515, no. 1–3, pp. 7–12, 2011, doi: 10.1016/j.cplett.2011.09.015.

[62] B. C. Smith, *Quantitative Spectroscopy: Theory and Practice*. Elsevier Science, 2003.

[63] M. Mecozzi, M. Pietroletti, and Y. B. Monakhova, “FTIR spectroscopy supported by statistical techniques for the structural characterization of plastic debris in the marine environment: Application to monitoring studies,” *Mar. Pollut. Bull.*, vol. 106, no. 1–2, pp. 155–161, 2016, doi: 10.1016/j.marpolbul.2016.03.012.

[64] P. Khare, B. P. Baruah, and P. G. Rao, “Application of chemometrics to study the kinetics of coal pyrolysis: A novel approach,” *Fuel*, vol. 90, no. 11, pp. 3299–3305, 2011, doi: 10.1016/j.fuel.2011.05.017.

[65] W. R. Ladner, “The products of coal pyrolysis: properties, conversion and reactivity,” *Fuel Process. Technol.*, vol. 20, no. C, pp. 207–222, 1988, doi: 10.1016/0378-3820(88)90021-5.

[66] R. C. Borah, P. Ghosh, and P. G. Rao, “A review on devolatilization of coal in fluidized bed,” *Int. J. Energy Res.*, vol. 35, no. 11, pp. 929–963, Sep. 2011, doi: 10.1002/er.1833.

[67] W. Li, Y. M. Zhu, C. Q. Hu, S. B. Han, and J. S. Wu, “Hydrocarbon Generation and Chemical Structure Evolution from Confined Pyrolysis of Bituminous Coal,” *ACS Omega*, vol. 5, no. 31, pp. 19682–19694, 2020, doi: 10.1021/acsomega.0c02352.

Acknowledgments

I would like to make specific acknowledgment of help received in paper writing and my study life in Tokushima university.

First, I would like to thank my supervisor, Yoshihiro Deguchi, for his guidance and patience. It would be impossible for me to finish my work without his kind help and valuable suggestions.

I also would like to thank researcher Takahiro Kamimoto and Professor Wang Zhenzhen. Their professionalism in performing experiments and paper writing have helped me a lot.

Wen Du and Cao Shengli have also contributed a lot in this work. They improved my manuscripts by offering valuable suggestions and Cao Shengli was my biggest assist in learning how to code.

Li Dichen and Shao Weidong also gave me great help in revising my manuscript. Special thanks to Li Dichen for inspiring me through the tough time.

Bumrungpon Mongkol also helped me in paper writing and gave me some good advice.

Ms. Muramoto have helped me dealing with paperwork and I am very grateful for her kind help.

Many thanks to all the lab members, many of them have already graduated and I cannot include all the names. They are all very kind people, and I would like to give them my many thanks.

Finally, I would like to thank my family, it is their love that support me all the time.